Kateřina Hlaváčková ORCID iD: 0000-0002-7218-8829
Olga Šamajová ORCID iD: 0000-0001-6121-7164
Miroslava Hrbáčková ORCID iD: 0000-0001-5039-6689
Jozef Šamaj ORCID iD: 0000-0003-4750-2123
Miroslav Ovečka ORCID iD: 0000-0002-1570-2174

Article Type: Original Article

Genetic manipulation of stress-induced mitogen-activated protein kinase modulates early stages of the nodulation process in *Medicago sativa*

Kateřina Hlaváčková[1], Olga Šamajová[1], Miroslava Hrbáčková[1], Jozef Šamaj[1], Miroslav Ovečka[1*]

[1]Department of Biotechnology, Faculty of Science, Palacký University Olomouc, Olomouc, Czech Republic

[*]**Correspondence:**
Miroslav Ovečka
email: miroslav.ovecka@upol.cz

Running title: SIMK modulates nodulation in alfalfa

One sentence summary: Genetic manipulation of SIMK in alfalfa revealed that SIMK modulates root hair capacity to form infection pockets and infection threads during the early interactions between alfalfa and rhizobia.

Total word count: 7191

Number of Figures: 9

Of which color: 9

Keywords: alfalfa, infection pocket, infection thread, MAPKs, nodulation, root hairs, SIMK, *Sinorhizobium meliloti*, subcellular localization

Abstract

Leguminous plants have established a mutualistic endosymbiotic interaction with nitrogen-fixing rhizobia to secure nitrogen sources in new specialized organs called root nodules. Before nodule formation, the development of early symbiotic structures is essential for rhizobia docking, internalization, targeted delivery, and intracellular accommodation. We have recently reported that overexpression of stress-induced mitogen-activated protein kinase (SIMK) in alfalfa affects root hair, nodule and shoot formation. However, detailed subcellular spatial distribution, activation, and developmental relocation of SIMK during the early stages of alfalfa nodulation remain unclear. Here, we qualitatively and quantitatively characterized SIMK distribution patterns in rhizobium-infected root hairs using live-cell imaging and immunolocalization, employing alfalfa stable transgenic lines with genetically manipulated SIMK abundance and kinase activity. In the *SIMKK-RNAi* line, showing downregulation of *SIMKK* and *SIMK*, we found a considerably decreased accumulation of phosphorylated SIMK around infection pockets and infection threads, which was strongly increased in the GFP-SIMK line, constitutively overexpressing GFP-tagged SIMK. Thus, genetically manipulated SIMK modulates root hair capacity to form infection pockets and infection threads. These results shed new light on SIMK spatio-temporal participation in the early interactions between alfalfa and rhizobia, and its internalization into root hairs, showing that local accumulation of active SIMK indeed modulates nodulation in alfalfa.

Introduction

Nitrogen shortage in the soil is one of the major factors restricting the growth and productivity of plants, including crops. To overcome or alleviate this limitation, *Medicago sativa* L. (alfalfa), a legume crop of high agronomic and ecological importance, is able to acquire nitrogen by symbiotic hosting of nitrogen-fixing rhizobia in *de novo* formed specialized organs, root nodules (Checcucci *et al.*, 2016; Wang *et al.*, 2018). Root nodules provide rhizobia with favorable conditions to convert atmospheric dinitrogen (N_2) into ammonia (NH_3) in the process of biological nitrogen fixation. Rhizobia export N-rich compounds to the host plant in exchange for carbohydrates that are utilized by rhizobia as a source of carbon and energy (White *et al.*, 2007; Oldroyd *et al.*, 2011). The legume-rhizobium symbiosis is established through a complex developmental process that starts with the exchange of signaling molecules between the host and symbiont, and the activation of signal transduction pathways, triggering the nodulation program in the host legume plant (Oldroyd, 2013; Yang *et*

al., 2022). Flavonoids secreted by legume roots regulate the transcriptional activity of nodulation (*nod*) genes that stimulate rhizobia to produce nodulation factors (NFs), lipochitooligosaccharides, with the backbone of N-acetylglucosamine units, and fatty acids at the non-reducing end. NFs are essential for host-specificity, rhizobial infection, and nodule organogenesis (Dénarié and Cullimore, 1993; Clúa *et al.*, 2018; Kidaj *et al.*, 2020). Perception of the correct NF structure by compatible receptors in legume root cells initiates early steps of nodulation. These early nodulation events include intracellular calcium oscillations, deformations of root hairs as well as alternations to the root hair cytoskeleton, preparing the host legume plant for symbiotic infection by invading rhizobia (Gage, 2004; Timmers, 2008; Roy *et al.*, 2020). Simultaneously, cell divisions in the root cortex and pericycle are reinitiated, leading to the establishment of root nodule primordium with active meristem (Jones *et al.*, 2007).

Nodule formation requires two separate, but spatially and temporally highly coordinated processes, namely rhizobial infection of root hairs and nodule organogenesis in the root cortex (Oldroyd and Downie, 2008; Ibáñez *et al.*, 2017). Before nodules arise as newly formed functional and nitrogen-fixing root lateral organs, rhizobia must travel from the root surface toward the target cells in the inner root tissue. In the initial stage, rhizobia attach to the growing root hair tips and are trapped in the root hair curls creating enclosed chambers, known as infection pockets (Fournier *et al.*, 2015; Rae *et al.*, 2021). Within the infection pockets, rhizobia divide and form colonies referred to as infection foci from which infection threads (ITs) entering root hairs are initiated by inverted tip growth. These plant-made tube-like membrane channels are filled with rhizobia, grow down towards the base of infected root hair, and branch out by growing through the root cortex. Eventually, the inward-growing IT and the outward-growing root nodule primordium meet inside the root tissue (Fournier *et al.*, 2008; Rashid *et al.*, 2015). When ITs reach the nodule primordium, rhizobia are released into the cytoplasm of host cells by endocytosis, become surrounded by plant-derived peribacteroid membrane, and differentiate into bacteroids that are responsible for nitrogen fixation by the activity of nitrogenase enzymatic complex (Terpolilli *et al.*, 2012; Poole *et al.*, 2018). Since only a specific NFs mixture allows a rhizobial strain to nodulate a particular legume host, mutual compatibility between the two symbionts is essential for establishing a successful symbiotic partnership (Wang *et al.*, 2018; Walker *et al.*, 2020).

Within a complex signaling network controlling the nodulation process, mitogen-activated protein kinases (MAPKs) become activated early after rhizobial infection (Lopez-

Gomez *et al.*, 2012). MAPK cascades represent conserved and universal signaling hubs transducing external stimuli into target substrates by a sequential action of three protein kinases, MAPK kinase kinase (MAPKKK), MAPK kinase (MAPKK), and MAPK. Plant MAPKs can be activated by a variety of biotic and abiotic stress stimuli. During signal transduction, MAPKKK reversibly activates its downstream MAPKK, which phosphorylates and activates MAPK by dual phosphorylation of threonine (T) and tyrosine (Y) residues of the T-X-Y motif (Pitzschke, 2015; Xu and Zhang, 2015; Zhang and Zhang, 2022). Activated MAPKs phosphorylate and regulate many diverse substrates such as transcription factors, enzymes, cytoskeletal proteins, or other kinases. Signaling through MAPK modules regulates a broad range of cellular and developmental processes as well as pathogenic or beneficial biotic interactions (Rasmussen *et al.*, 2012; Šamajová *et al.*, 2013; Smékalová *et al.*, 2014; Komis *et al.*, 2018; Sun and Zhang, 2022).

Although MAPK-mediated phosphorylation cascades represent an essential component of plant cell signaling, still relatively little is known about MAPKs in legume crops. In alfalfa, stress-induced MAPK (SIMK) is activated by biotic and abiotic stimuli such as fungal elicitors and salt stress, respectively (Munnik *et al.*, 1999; Cardinale *et al.*, 2000, 2002). Activation analyses and yeast two-hybrid screening identified SIMK kinase (SIMKK) as SIMK specific activator. SIMKK directly activates SIMK in response to salt stress (Kiegerl *et al.*, 2000; Cardinale *et al.*, 2002) and localization studies at the subcellular level revealed substantial relocation of both SIMKK and SIMK from nuclei to the cytoplasmic spot-like compartments upon salt stress (Ovečka *et al.*, 2014). In addition, activated SIMK relocates from nuclei to the tips of growing root hairs and together with the dynamic actin cytoskeleton regulates alfalfa root hair tip growth (Šamaj *et al.*, 2002, 2003). Most importantly, we have recently addressed SIMK positive role in alfalfa nodulation and development through its genetic manipulations. For this functional assessment, a transgenic *SIMKK-RNAi* line with a strong downregulation of SIMK production and activity, and a transgenic GFP-SIMK line constitutively overexpressing GFP-tagged and activated SIMK were utilized. SIMK overexpression promoted root hair growth, ITs and nodules clustering, as well as positively affected agronomical traits such as shoot biomass production, suggesting the biotechnological potential of this kinase (Hrbáčková *et al.*, 2021). However, the functional and spatiotemporal mode of SIMK participation at early nodulation stages remains unknown.

In this study, live-cell imaging using light-sheet fluorescence microscopy supplemented with quantitative microscopy employing alfalfa-adapted immunolabeling

techniques revealed SIMK-specific subcellular localization and activation at early stages of alfalfa – *Sinorhizobium meliloti* symbiotic interaction process. SIMK in root hairs targeted the docking site where *S. meliloti* was attached, entrapped, and internalized. We correlated SIMK subcellular localization patterns in root hairs at *S. meliloti* internalization sites in two contrasting alfalfa genotypes, stably overexpressing GFP-tagged SIMK and downregulating SIMK level by means of *SIMKK* RNAi technology, respectively. SIMK genetic manipulation, the mode of activation, and the localization pattern indicate that the effectiveness of early nodulation steps in alfalfa is modulated by precise spatiotemporal SIMK localization and activation.

Results

SIMK distribution in alfalfa growing root hairs

To characterize SIMK localization patterns in growing root hairs of alfalfa control and transgenic plants, whole-mount immunofluorescence analysis after plant fixation was performed. Under control conditions, when alfalfa root hairs were not exposed to *S. meliloti*, a tip-focused pattern of SIMK distribution was observed (Figure 1). Immunodetection revealed mainly apical and sub-apical localization of SIMK in growing root hairs of alfalfa RSY plants (Figure 1A) and plants of transgenic *SIMKK-RNAi* (Figure 1D) and GFP-SIMK (Figure 1G) lines. Moreover, the activated pool of MAPKs in root hairs of RSY (Figure 1B), *SIMKK-RNAi* (Figure 1E) and GFP-SIMK (Figure 1H) plants were spatially detected, showing the same distribution (Figure 1, C, F, I). GFP localization in fixed root hairs of transgenic GFP-SIMK line confirmed the SIMK localization pattern obtained by immunolabeling (Figure 1, G and J). Profiling of fluorescence intensity distribution along individual root hairs was documented by semi-quantitative measurements showing higher accumulation of SIMK and activated MAPKs in the apex and sub-apex of alfalfa root hairs (Figure 1, K-P). In comparison to RSY root hairs (Figure 1, K and L), the displayed profile distribution revealed decreased fluorescence intensity of both SIMK and activated MAPKs in root hair tips of transgenic *SIMKK-RNAi* line (Figure 1, M and N), while the fluorescence intensity of both SIMK and activated MAPKs was increased in root hair tips of transgenic GFP-SIMK line overexpressing GFP-tagged SIMK (Figure 1, O and P). These results demonstrate a considerably decreased presence of activated SIMK in root hair tips of transgenic *SIMKK-RNAi* line compared to RSY, while it was considerably increased in overexpression GFP-

SIMK lines. Since root colonization by *S. meliloti* initiates from growing root hairs, the presence of activated SIMK in the root hair tip may be an essential component of initial attachment and invasion steps by rhizobia and could be potentially required for the establishment and efficient formation of early symbiotic structures.

The reaction of GFP-SIMK to rhizobia infection

To characterize the GFP-SIMK localization pattern during early nodulation stages *in vitro*, live cell imaging of alfalfa roots stably expressing GFP-tagged SIMK, co-cultivated with mRFP-labeled *S. meliloti* was performed by LSFM 3 to 4 days post inoculation (dpi) (Figure 2A). The mode of interaction was analyzed in the mature part of roots, typically involved in nodulation, where GFP-SIMK is no more accumulated at the tip of root hairs because of terminated tip growth (Figure 2, A and B). GFP-SIMK at this stage is located mainly in nuclei and cytoplasm of root hairs (Hrbáčková *et al.*, 2021). Roots inoculated with *S. meliloti* were cultivated on the surface of agar plates, leading to the formation of a dense layer-like biofilm of mRFP-labeled *S. meliloti* associated only with the root and root hairs touching the agar surface. This model allows studying simultaneously and independently root hairs symbiotically interacting with rhizobia, but also root hairs untouched by rhizobia that were exposed to air inside the Petri dish. Both types of root hairs are present on the same root exposed to the same conditions and treatments (Figure 2A). Therefore, 3D rendering of symbiotically infected GFP-SIMK root enabled us to distinguish not only non-interacting alfalfa root hairs from those that interact with rhizobia but also the position of their nuclei with respect to infection (Supplemental Movie S1). In non-growing root hairs that were not in physical contact with rhizobia, nuclei were positioned almost uniformly near the root hair base (Figure 2B; Supplemental Movie S1) while in reactivated root hairs under symbiotic interaction, nuclei were located closer to the site of rhizobia attachment at the tip (Figure 2C; Supplemental Movie S1). Preference for detailed LSFM live-cell imaging was given to the curled root hairs with attached rhizobia (Figure 2D) or rhizobia already enclosed in the root hair curls (Figure 2, E and F), for characterization of SIMK involvement in early infection structures.

Rhizobia-induced GFP-SIMK subcellular relocation

To find out whether exposure of alfalfa plants to beneficial rhizobia leads to changes in GFP-SIMK distribution that could be related to the early symbiotic infection, the mean

fluorescence intensity of GFP-SIMK was quantitatively evaluated in non-interacting (Figure 3A) and rhizobia-interacting (Figure 3B) root hairs. Under control conditions, GFP-SIMK was present in nuclei and root hair tips of non-interacting root hairs. Nevertheless, a higher amount of GFP-SIMK was detected in nuclei (Figure 3C). During early nodulation stages, GFP-SIMK was localized in nuclei, but substantial accumulation occurred also around rhizobia at specific infection sites (Figure 3B). Upon this early rhizobial infection, the amount of GFP-SIMK in nuclei decreased compared to control conditions (Figure 3 D and E). It seems that GFP-SIMK rather redistributes in root hairs upon rhizobia interaction and accumulates at infection sites where the nodulation process begins (Figure 3, B and D). This finding further suggests the supportive role of SIMK during the early stages of alfalfa nodulation.

Association of GFP-SIMK with rhizobia infection sites

Detailed live cell imaging of symbiotically-interacting root hairs revealed localization of GFP-SIMK and its association with the position of fluorescently labeled *S. meliloti* at individual early infection stages, beginning from rhizobia attachment (Figure 4A), rhizobia entry into the root hairs (Figure 4, B and C), infection pocket formation (Figure 4D) up to rhizobia complete enclosure inside infection pockets (Figure 4E). The first morphological response to attached rhizobia was root hair curling (Figure 4F). Semi-quantitative evaluation of GFP-SIMK fluorescence intensity distribution showed increased accumulation of GFP-SIMK in the apex of curled root hair, but also at a specific site of rhizobia attachment (Figure 4, F and G). Moreover, orthogonal projections revealed a very close association of GFP-SIMK with rhizobia attached to the root hair at this specific infection site in the X-Z view (Figure 4H; Supplemental Movie S2 at 0:00:14s–0:00:21s) and the Y-Z view (Figure 4I; Supplemental Movie S3 at 0:00:14s–0:00:21s). Later upon infection, a cluster of rhizobia was located specifically at the neck of root hair curl where rhizobia will enter the root hair (Figure 4J). Profile measurements revealed an accumulation of GFP-SIMK in the nucleus located close to the infection site, its relocation from the apex, and specific accumulation at the infection site (Figure 4, J and K). Orthogonal projections from the X-Z view (Figure 4L; Supplemental Movie S4 at 0:00:14s–0:00:18s) and the Y-Z view (Figure 4M; Supplemental Movie S5 at 0:00:16s–0:00:24s) revealed close association of GFP-SIMK with rhizobia gathered at the root hair curl through which rhizobia internalization typically takes place. Before rhizobia entry into the alfalfa root hairs, a stage of very tight contact between the

curled root hair tip and entrapped rhizobia was captured by LSFM (Figure 4N). Profile measurements showed increased fluorescence intensity of GFP-SIMK at the site where rhizobia are in very close contact with the root hair (Figure 4, N and O). Observation of very tight association including the partial overlay was confirmed from orthogonal projections in the X-Z view (Figure 4P; Supplemental Movie S6 at 0:0014s–0:00:21s) and the Y-Z view (Figure 4Q, Supplemental Movie S7 at 0:00:15s–0:00:24s). Once were individual rhizobia entrapped inside root hair curl, an infection pocket formation was initiated (Figure 4R). GFP-SIMK was found to be accumulated around rhizobia surrounding them inside root hair curls (Figure 4S) and associated with them as shown from orthogonal projections in the X-Z view (Figure 4T; Supplemental Movie S8 at 0:00:13s–0:00:25s) and the Y-Z view (Figure 4U; Supplemental Movie S9 at 0:00:14s–0:00:22s). Later, rhizobia divide and form colonies within infection pockets (Figure 4V) from which ITs are subsequently initiated. GFP-SIMK was strongly accumulated around infection pockets containing rhizobia (Figure 4W) and orthogonal projections in the X-Z view (Figure 4X; Supplemental Movie S10 at 0:00:15s–0:00:22s) and the Y-Z view (Figure 4Y; Supplemental Movie S11 at 0:00:14s–0:00:21s) corroborated close GFP-SIMK distribution around infection pockets. Importantly, *in vivo* time-lapse imaging showed that accumulation of GFP-SIMK at the infection site in root hairs during rhizobia attachment (Supplemental Movie S12) and around infection pockets (Supplemental Movie S13) is stable over time, as semi-quantitatively documented profile measurements of GFP-SIMK fluorescence intensity distribution did not fluctuate (Supplemental Movie S14 and S15). Altogether, live cell LSFM imaging showed specific localization and accumulation of GFP-SIMK at infection sites during the early infection stages, which very closely associated with attaching and internalizing rhizobia. Based on the presence of activated SIMK in the growing tips of alfalfa root hairs (Figure 1), it seems that accumulation and activation of SIMK might play an important role in the early stages of alfalfa root hair infection by *S. meliloti*.

SIMK subcellular localization during infection pockets formation

To reveal the subcellular localization pattern of SIMK and activated MAPKs in root hairs of control RSY and transgenic *SIMKK-RNAi* and GFP-SIMK plants 3-7 dpi with *S. meliloti*, and their association with infection pockets, immunofluorescence localization microscopy was employed. Fixed root samples were immunolabeled for SIMK and activated MAPKs using SIMK-specific and phospho-specific antibodies, respectively. The pattern of SIMK and

252 activated MAPK localization was documented in infection pockets, the first symbiotic
253 structure, formed inside root hairs after rhizobial internalization. DAPI, typically used for
254 DNA nuclear staining, effectively stained also *S. meliloti*, which enabled a detailed study of
255 MAPKs association with intracellular compartments enclosing rhizobia during the early
256 stages of the nodulation process. Upon root hair curling, *S. meliloti* was entrapped in alfalfa
257 root hair curls and became completely enclosed inside infection pockets (Figure 5A). At this
258 symbiotic stage, immunostaining revealed SIMK localization close to the plasma membrane
259 and particularly prominent SIMK-specific accumulation around infection pockets in the
260 alfalfa RSY line (Figure 5B). Labeling of activated MAPKs showed the same pattern of
261 localization (Figure 5C), indicating a colocalization with SIMK-specific signal (Figure 5D).
262 This suggests that MAPKs localized around infection pockets were phosphorylated.
263 Moreover, a semi-quantitative evaluation of fluorescence intensity distribution confirmed the
264 close association of both SIMK and activated MAPKs with infection pockets (Figure 5P).

265 In root hairs of the transgenic *SIMKK-RNAi* line, infection pockets filled with DAPI-stained *S.*
266 *meliloti* (Figure 5E) were surrounded by a very faint signal of both SIMK (Figure 5F) and
267 activated MAPKs (Figure 5G), showing a similar pattern of localization (Figure 5H). Semi-
268 quantitative profile measurements revealed an association of SIMK and activated MAPKs
269 with infection pockets. However, compared to the alfalfa RSY plants (Figure 5P), the
270 fluorescence intensity of SIMK and activated MAPKs was substantially decreased in the
271 transgenic *SIMKK-RNAi* line (Figure 5Q).

272 Similarly, inside root hairs of transgenic GFP-SIMK line, when *S. meliloti* became fully
273 entrapped inside infection pockets (Figure 5I), immunodetection with SIMK-specific antibody
274 revealed substantial accumulation mainly around infection pockets, but prominent SIMK-
275 specific signal was also detected at the plasma membrane of curled root hairs (Figure 5J).
276 Activated MAPKs showed a similar subcellular localization pattern around infection pockets
277 and at the plasma membrane of curled root hairs (Figure 5K), leading to a high degree of
278 colocalization with SIMK-specific signal (Figure 5L). SIMK localization pattern obtained by
279 immunostaining with SIMK-specific antibody was independently confirmed by localization of
280 GFP-tagged SIMK in curled root hairs of the GFP-SIMK line (Figure 5M). Also, GFP-tagged
281 SIMK showed a high degree of colocalization with SIMK signal obtained by immunolabeling
282 with SIMK-specific antibody (Figure 5N), and semi-quantitative evaluation of SIMK and
283 activated MAPKs fluorescence intensity distribution clearly revealed its close association
284 with infection pockets (Figure 5, O and R).

In addition, quantitative comparative analysis of mean fluorescence intensity around infection pockets revealed, in comparison to control RSY (Figure 6, A and G), significantly higher levels of SIMK in GFP-SIMK plants (Figure 6, C and G) and significantly lower in transgenic *SIMKK-RNAi* line (Figure 6, B and G). Also, a lower level of activated MAPKs was found around infection pockets inside root hairs of the transgenic *SIMKK-RNAi* line (Figure 6, E and H), while no significant difference was observed in the transgenic GFP-SIMK line compared to alfalfa RSY plants (Figure 6, D, F and H).

Quantitative determination of the colocalization rate between signals of SIMK and activated MAPKs, expressed by Pearson's correlation coefficient, revealed the highest value around infection pockets in the transgenic GFP-SIMK line, and the lowest in transgenic *SIMKK-RNAi* line (Supplemental Figure S1).

This analysis clearly showed SIMK-specific accumulation and activation around infection pockets containing entrapped *S. meliloti* in alfalfa root hairs. The level of active SIMK accumulation was strongly associated with the SIMK expression level. It was substantial in root hairs of the transgenic GFP-SIMK line, while the lowest presence of active SIMK was detected around infection pockets in the transgenic *SIMKK-RNAi* line causing strong downregulation of both *SIMKK* and *SIMK* (Hrbáčková *et al.*, 2021). Since infection pockets represent the site of *S. meliloti* entry and ITs initiation, these results indicate that active SIMK accumulated at this specific location might be required for efficient ITs formation.

SIMK subcellular localization during ITs formation

Complete enclosure of rhizobia inside infection pockets is followed by an invagination of the host cell plasma membrane and initiation of tunnel-like ITs. Therefore, the pattern of SIMK and activated MAPKs subcellular localization was characterized by immunolabeling during ITs formation and propagation through root hairs. Inside root hairs of the alfalfa RSY line, ITs were easily detectable owing to DAPI-stained *S. meliloti* (Figure 7A). Immunostaining revealed SIMK-specific signals surrounding growing ITs (Figure 7B). Activated MAPKs immunolabeled with anti-phospho-p44/42 antibody showed the same subcellular distribution (Figure 7C) leading to a high degree of colocalization with the SIMK signal (Figure 7D). This colocalization pattern suggests that SIMK located around ITs was phosphorylated. Semi-quantitative analysis of the fluorescence intensity distribution revealed a close association of both SIMK and activated MAPKs with the surface of infection threads (Figure 7O).

316 In the transgenic *SIMKK-RNAi* line, ITs filled with *S. meliloti* (Figure 7E) were similarly
317 decorated by MAPKs, but showed a very weak signal of both SIMK (Figure 7F) and activated
318 MAPKs (Figure 7G). Nevertheless, the distribution pattern indicated their subcellular
319 colocalization (Figure 7H). Profiling of SIMK and activated MAPKs fluorescence intensity
320 distribution revealed their association with ITs, but substantially decreased (Figure 7P).

321 In the case of ITs in the transgenic GFP-SIMK line (Figure 7I), immunostaining with SIMK-
322 specific antibody revealed a strong accumulation of SIMK not only along ITs, but also at the
323 plasma membrane of root hairs (Figure 7J). Signal specific for activated MAPKs showed the
324 same pattern of subcellular localization (Figure 7K) and colocalized with SIMK signal
325 (Figure 7L). Observation of GFP-tagged SIMK along ITs (Figure 7M) confirmed the
326 localization pattern obtained by immunolabeling with SIMK-specific antibody and
327 colocalized with SIMK signal (Figure 7N). Semi-quantitative evaluation of fluorescence
328 intensity along indicated profiles (Figure 7, L and N) confirmed enhanced and close
329 association of SIMK and activated MAPKs with ITs and plasma membrane of root hairs
330 (Figure 7, Q and R).

331 Moreover, the amount of SIMK (Figure 8, A-C) and activated MAPKs (Figure 8, D-F)
332 determined by quantitative analysis of mean fluorescence intensity around ITs was markedly
333 lower in plants of transgenic *SIMKK-RNAi* line in comparison to alfalfa RSY and GFP-SIMK
334 plants (Figure 8, G and H), while the amount of activated MAPKs in transgenic GFP-SIMK
335 line was similar to RSY plants (Figure 8H).

336 The colocalization rate between SIMK and activated MAPKs was quantitatively determined
337 by Pearson's correlation coefficient, revealing that the overall colocalization rate between
338 SIMK and activated MAPKs was significantly higher along ITs in the transgenic GFP-SIMK
339 line and RSY plants compared to the transgenic *SIMKK-RNAi* plants (Supplemental Figure
340 S2).

341 Immunolocalization together with semi-quantitative and quantitative colocalization analyses
342 clearly revealed the presence of SIMK-specific signal along ITs in alfalfa root hairs. Increased
343 accumulation of active SIMK along ITs was observed in the transgenic GFP-SIMK line,
344 while the lowest one was detected in the *SIMKK-RNAi* line. All these data indicate that active
345 SIMK might be involved during ITs formation and its growth toward the place of root nodule
346 primordia initiation. Therefore, SIMK supportive role in the propagation of rhizobia-filled ITs

through plant root hairs and cortex tissues might play an important role in the regulation and effectiveness of rhizobia delivery to the nodule primordium and subsequent nodule formation.

Moreover, we performed a visualization of plasma membranes using a fixable FM4-64FX, allowing precise observation of SIMK subcellular localization with regard to membranes of early symbiotic structures. Whole-mount immunofluorescence co-labeling in RSY revealed the presence of SIMK close to the membranous surface of infection pockets (Figure 9, A and C) and ITs (Figure 9, B and D). A lower amount of SIMK was found on membranes of infection pockets (Figure 9, E and G) and ITs (Figure 9, F and H) in the *SIMKK-RNAi* line, while a substantially increased amount of SIMK was accumulated on the surface of infection pockets (Figure 9, I and K) and ITs (Figure 9, J and L) in GFP-SIMK line. In quantitative terms, Pearson's correlation coefficient showed the highest colocalization rate between SIMK and FM4-64FX-labeled membranes in the GFP-SIMK line, while the degree of colocalization was considerably decreased in the *SIMKK-RNAi* line (Figure 9M). The data suggest a close association and interaction of SIMK with membranes of infection pockets and ITs during early nodulation stages.

Involvement of active SIMK in ITs formation

To correlate the presence of active SIMK at infection pockets and ITs with nodule formation, the efficiency of root hair infection by *S. meliloti* was examined. The number of ITs per the whole root system length was determined in alfalfa RSY and transgenic *SIMKK-RNAi* and GFP-SIMK plants at 10 dpi with *S. meliloti*, when actively growing ITs should already reach the root cortex. No significant difference was observed in the averaged root system length among the three respective lines at 10 dpi with *S. meliloti* (Supplemental Figure S3A). However, the transgenic *SIMKK-RNAi* line, having strongly downregulated both *SIMKK* and *SIMK* (Hrbáčková *et al.*, 2021), showed the lowest amount of active SIMK around infection pockets (Figure 6, E and H, Figure 9, E,G,M), formed significantly fewer ITs compared to RSY and transgenic GFP-SIMK plants, while the transgenic GFP-SIMK line produced a similar number of ITs as RSY plants (Supplemental Figure S3B).

Discussion

Leguminous plants are immensely important to the ecosystem and sustainable agriculture worldwide. Part of their success lies in mutualistic partnership with beneficial nitrogen-fixing

bacteria that can convert atmospheric dinitrogen into bioavailable ammonium inside functional root nodules, which helps them to manage nitrogen shortage and facilitate nutrient uptake (Brundrett, 2002; Bisseling and Geurts, 2020). Alfalfa has become a high-quality forage crop with high biological and agronomical potential, especially for its widespread production, ecological adaptability, high nutrition value, and ability to improve nitrogen-limited soils (Radović *et al*., 2009). Early steps of nodulation and subsequent nodule development depend on a molecular dialogue between the host legume and rhizobia, including the exchange of signals and activation of protein-phosphorylation-mediated signal transduction cascades (Shaw and Long, 2003; Grimsrud *et al.*, 2010). Specifically in plants, developmental and cellular processes are regulated by MAPK-mediated phosphorylation cascades, and the activity of various protein kinases was shown to be also involved in symbiotic interactions and nodule formation (Grimsrud *et al.*, 2010; Komis *et al.*, 2018; Roy *et al.*, 2020). Although symbiotic nitrogen fixation is extensively studied in model legume species, such as *Medicago truncatula* and *Lotus japonicus*, little is known about the regulation of symbiotic interaction and the possible involvement of MAPK signaling in alfalfa nodulation. Here, we characterized the subcellular localization and activation pattern of SIMK involved in the early stages of alfalfa interaction with *Sinorhizobium meliloti* using genetically engineered transgenic lines.

Despite the remarkable progress in the understanding of MAPK regulation in plant development and immunity, their involvement in various steps of nodule development is still not known. In *L. japonicus*, a MAPKK SIP2 was identified to interact with a symbiosis receptor-like kinase (SymRK), having an essential role in early symbiotic signaling (Chen *et al.*, 2012). Yin *et al.* (2019) identified LjMPK6 as the phosphorylation target of SIP2 and showed that the SymRK-SIP2-LjMPK6 signaling module is required for nodule organogenesis and formation in *L. japonicus*. In addition, a recent study demonstrated that LjPP2C, a type 2C protein phosphatase, fine-tunes nodule development in *L. japonicus* via dephosphorylating LjMPK6 (Yan *et al*., 2020). In *M. truncatula*, MtMAPKK4 shows a high sequence identity to MsSIMKK and LjSIP2. Downstream interacting partners of MtMAPKK4 are MtMAPK3 and MtMAPK6, while the MtMAPKK4-MtMAPK3/6 pathway is involved in nodule formation and also with *M. truncatula* general growth and development (Chen *et al.*, 2017). Another MAPKK from *M. truncatula*, MtMAPKK5, directly activates MtMAPK3 and MtMAPK6, and the stress signaling-mediated MtMAPKK5-MtMAPK3/6 module negatively affects root nodulation (Ryu *et al.,* 2017). In alfalfa, SIMKK is a specific upstream activator

of SIMK under salt stress (Kiegerl *et al*., 2000) and both SIMKK and SIMK relocate from the nucleus to cytoplasm under salt stress (Ovečka *et al*., 2014). SIMK overexpression leads to the development of longer root hairs and promoted ITs and nodule clustering (Hrbáčková *et al*., 2021). In contrast, SIMK downregulation was accompanied by the formation of shorter root hairs and few ITs and nodules. Moreover, SIMK overexpression promoted shoot biomass production, and leaf and petiole development. However, a detailed study of SIMK subcellular localization and activation pattern clarifying the spatial and temporal model of SIMK involvement in alfalfa early nodulation stages remained unclear.

Possible SIMK involvement in alfalfa nodulation can be anticipated from its subcellular localization and activation during early symbiotic stages. Crucial is the very tight association of activated SIMK with infection pockets and ITs. We have recently established light-sheet fluorescence microscopy for the spatiotemporal imaging of plant development at subcellular, cellular, tissue and organ levels under controlled environmental conditions (Ovečka *et al*., 2018). It was utilized in alfalfa for the characterization of root development (Vyplelová *et al*., 2018) and the involvement of actin cytoskeleton in the interaction with *S. meliloti* (Ovečka *et al*., 2022). Live-cell imaging using LSFM clearly showed relocation of SIMK from root hair tips to the *S. meliloti* docking site and further close association with sites of rhizobia internalization. We developed also reliable immunolocalization protocols for whole-mount immunolabeling of root samples of *M. sativa*, achieving high signal efficiency and superb sample stability (Tichá *et al*., 2020). Employing these immunolabeling methods explicitly adapted for alfalfa plantlets originating from somatic embryos, we show here subcellular localization patterns of SIMK during the early stages of the nodulation process in alfalfa. Moreover, immunolocalization of phosphorylated MAPKs enabled us to check out whether SIMK is activated or not at the subcellular level. Under control conditions, alfalfa RSY plants and plants of transgenic *SIMKK-RNAi* and GFP-SIMK lines showed a tip-focused pattern of activated SIMK localization in growing root hairs in agreement with previously published data on SIMK localization from both live-cell imaging (Hrbáčková *et al*., 2021) and immunofluorescence microscopy (Šamaj *et al*., 2002). However, decreased accumulation of activated SIMK in growing root hair tips was observed in the transgenic *SIMKK-RNAi* line, consistent with Bekešová *et al*. (2015) showing overall decreased accumulation of phosphorylated SIMK in *SIMKK-RNAi* lines. Although rhizobia can use different routes to invade plant roots, entrance via root hairs is probably the best understood and could be found in legumes such as alfalfa, soybean, pea, bean and vetch (Sprent and James, 2007; Sprent *et*

al., 2008; Ibáňez *et al.*, 2017). Since root hairs make the first contact with symbiotic rhizobia, active SIMK in root hairs may play an important role in the alfalfa's early interaction with *S. meliloti* during and after rhizobia attachment. Activation of signaling pathways in the epidermal cells leads to localized inhibition of the tip growth of root hairs and induces its physical curling around attached rhizobia. It is followed by the formation of infection pockets and infection threads, structures essential for rhizobia internalization and delivery toward the target cells in newly forming nodules (Brewin, 2004; Gage 2004). In contrast to the overexpressor GFP-SIMK line, where activated SIMK was strongly accumulated around infection pockets and ITs, the transgenic *SIMKK-RNAi* line showed much-decreased accumulation. Indeed, the number of formed ITs was significantly lower in the transgenic *SIMKK-RNAi* line, indicating the importance of activated SIMK in infection pockets, which is further required for proper ITs formation. Therefore, SIMK downregulation negatively affects nodule formation, while SIMK overexpression enhances infection pockets and ITs formation.

Conclusively, we show that active SIMK is associated with *S. meliloti* internalization sites in root hairs and with ITs delivering *S. meliloti* to internal root tissues. SIMK downregulation negatively affects infection pockets and ITs formation. The subcellular immunolocalization pattern supported by the localization pattern of GFP-SIMK in living cells thus clearly demonstrates that active SIMK might be a key player responsible for fine-tuning of the nodulation process in alfalfa. SIMK, therefore, represents a potentially new regulatory protein required for the establishment of efficient symbiotic interaction in alfalfa.

Materials and methods

Plant material

Alfalfa wild-type plants of cv. Regen-SY (RSY) carrying either *35S::GFP:SIMK* construct (GFP-SIMK fusion protein; Hrbáčková *et al.*, 2021) or *SIMKK-RNAi* in pHellsgate12 plasmid driven under *35S* promoter (obtained from CSIRO Plant Industry, Australia) were obtained by regeneration *in vitro* through somatic embryogenesis from leaf explants as previously described (Samac and Austin-Phillips, 2006; Bekešová *et al.*, 2015; Hrbáčková *et al.*, 2021). Regenerated alfalfa plants RSY, transgenic *SIMKK-RNAi* line (showing strong downregulation of *SIMKK* and *SIMK* transcripts and SIMK protein), and transgenic GFP-SIMK line with upregulated *SIMK* transcript and enhanced SIMK activity (Hrbáčková *et al.*,

2021) were transferred to nitrogen-free Fåhreus medium (FAH-N_2; Fåhreus, 1957) for inoculation with rhizobia.

Plant inoculation with S. meliloti

Regenerated plantlets of transgenic GFP-SIMK line approximately 1.5 cm long and growing on a FAH-N_2 medium containing 13 g/L of micro agar were inoculated with *S. meliloti* (strain Sm2011) producing mRFP with OD_{600}= 0.5 (2.50e+008 cell/ml) and used for live-cell imaging 3 to 4 dpi. For quantitative analyses, 18 days old plants of alfalfa RSY and transgenic *SIMKK-RNAi* and GFP-SIMK lines originating from somatic embryos and growing on the FAH-N_2 medium were inoculated with *S. meliloti* wild-type (strain Sm2011) with OD_{600}= 0.5. In total, 2 ml of rhizobial suspension was applied to the root system directly on plates, followed by vertical cultivation of inoculated plants in an environmental chamber at 21°C, 70% humidity, and 16h/8h light/dark cycle with covered root systems.

Sample preparation for live-cell imaging and light-sheet fluorescence microscopy (LSFM)

Plantlets of transgenic GFP-SIMK line were used for live cell imaging to observe *in vivo* localization and dynamics of GFP-tagged SIMK during the early stages of nodulation. Samples for LSFM imaging were prepared according to Ovečka *et al*., 2015. Fluorinated ethylene propylene (FEP) tube with an inner diameter of 4.2 mm and outer diameter of 4.6 mm was connected to the glass capillary (inner diameter of 2.15 mm and outer diameter of 4.0 mm) using the hot glue gun. Inoculated plantlet was gently inserted into the FEP tube with tweezers and medium (FAH-N_2 medium pH 6.5) with 1% (w/v) low melting point agarose (Sigma Aldrich) containing fiducial markers (fluorescent beats of 1 µm in diameter) was slowly added from the bottom into the FEP tube. Under these conditions, the plant root was embedded in the solidified block of the culture medium inside the FEP tube while the green upper part of the plant was exposed to air. The glass capillary connected to the FEP tube containing the embedded sample was fixed into the metal holder and directly placed into a pre-tempered (22°C) LSFM observation chamber filled with a liquid FAH-N_2 medium. After sample stabilization, imaging was performed using the light-sheet Z.1 fluorescence microscope (Carl Zeiss, Germany) equipped with Plan-Apochromat 10×/0.5 NA detection objective and two LSFM 10×/0.2 NA illumination objectives (Carl Zeiss, Germany). Rhizobia-infected roots were imaged using dual-side light-sheet illumination with excitation

laser lines 488 nm for GFP (beam splitter LP 560 and emission filter BP 505-545) and 561 nm for RFP (beam splitter LP 560 and emission filter BP 575-615). Images were acquired with the PCO.Edge sCMOS cameras (PCO AG, Germany) with an exposure time of 50 ms and an imaging frequency of every 2 min in Z-stack mode for 80 and 120 min. The scaling of acquired images in x, y, and z dimensions was 0.466 µm × 0.466 µm × 1.497 µm, and light-sheet thickness was set to the optimal value.

Fixation of alfalfa root samples

For whole-mount immunofluorescence labeling, approximately 1.5 cm long root segments were excised from roots of alfalfa RSY, *SIMKK-RNAi* and GFP-SIMK plants co-cultivated with *S. meliloti* and fixed in freshly prepared fixative solution (Tichá *et al.*, 2020). Sampling was done at 3-7 dpi with *S. meliloti* when infection pockets and growing ITs were clearly detectable inside rhizobia-infected root hairs after microscopic observation.

Immunolabeling of SIMK and activated MAPKs in symbiotically-infected root hairs

SIMK subcellular localization at early symbiotic stages was performed by immunofluorescence labeling on fixed root samples of alfalfa RSY, *SIMKK-RNAi* and GFP-SIMK lines co-cultivated with *S. meliloti* using a SIMK-specific antibody. To check out the activation state of SIMK in analyzed early stages of nodulation, an activated pool of MAPKs was immunodetected using a phospho-specific antibody (anti-phospho-p44/42, Cell Signaling, Netherlands). Root samples were simultaneously double-immunolabeled with rabbit anti-AtMPK6 (SIMK-specific) primary antibody (Sigma, Life Science, USA) at 1:750 dilution in 2.5% (w/v) BSA in phosphate-buffered saline [PBS; 140 mM NaCl, 2.7 mM KCl, 6.5 mM $Na_2HPO_4 \times 2H_2O$, 1.5 mM KH_2PO_4, pH 7.3] for SIMK localization and with mouse anti-phospho-p44/42 primary antibody at 1:400 dilution in 2.5% (w/v) BSA in PBS to visualize activated MAPKs. To improve antibody penetration, vacuum infiltration was used (3×5 min), followed by overnight incubation at 4°C. Samples were then sequentially incubated with appropriate Alexa Fluor-conjugated secondary antibodies. First, Alexa Fluor 647 rabbit anti-mouse secondary antibody (Abcam) diluted 1:500 in 2.5% (w/v) BSA in PBS was used for 2h incubation at 37°C. Samples were extensively washed in PBS (5×10 min), blocked in 5% (w/v) BSA in PBS for 20 min at RT, and incubated with Alexa Fluor 555 goat anti-rabbit secondary antibody (Abcam) by keeping the same dilution and incubation

conditions. Nuclei and *S. meliloti* were visualized with 1 $\mu g \cdot ml^{-1}$ DAPI diluted 1:1000 in PBS for 15 min at RT in darkness.

FM4-64 staining

The fixable variant of the styryl dye FM4-64 (FX) was used for *in situ* visualizations of plasma membranes in alfalfa root cells treated with *S. meliloti*. Roots were labeled in liquid FAH-N_2 medium (pH 6.5) containing FM4-64 (FX) at a final concentration of 4 µM in 5 ml Eppendorf tubes for 20 min. The whole labeling was performed on ice. The excess dye was quickly washed out with liquid FAH-N_2 medium, roots were cut into 1.5 cm long segments and immediately fixed as described previously (Tichá *et al*., 2020). Fixed root segments were used for immunolabeling as described above. For SIMK immunostaining in FM4-64 (FX)-labeled samples, rabbit SIMK-specific primary and Alexa Fluor 647 goat anti-rabbit secondary antibodies were used.

Confocal laser scanning microscopy (CLSM) and Airyscan CLSM

Root samples immunolabeled for SIMK and activated MAPKs were mounted in the antifade mounting medium [0.1% (w/v) paraphenylenediamine in 90% (v/v) glycerol buffered with 10% (v/v) PBS at pH 8.2 - 8.6] to protect samples from photo-bleaching and used for microscopy. Imaging of immunolabeled SIMK and activated MAPKs was performed with Zeiss LSM 710 platform (Carl Zeiss, Germany) equipped with Plan-Apochromat 40×/1.4 Oil DIC M27 and Plan-Apochromat 63×/1.4 Oil DIC M27 objectives. Samples were imaged with excitation laser lines at 405 nm for DAPI, 488 nm for detection of GFP, 561 nm for Alexa Fluor 555 to visualize SIMK and 631 nm for Alexa Fluor 647 to detect activated MAPKs. Microscopic analysis of immunostained SIMK and FM4-64 FX-visualized membranes in rhizobia-infected root hairs was performed with a Zeiss LSM 880 Airyscan equipped with 32 GaAsP detectors (Carl Zeiss, Germany) using a Plan-Apochromat 63×/1.4 Oil DIC M27 objective. Samples were imaged with excitation laser lines at 561 nm for FM4-64FX and 631 nm for Alexa Fluor 647.

Quantification of ITs

For quantitative evaluation of ITs formation, 18 days old plants of RSY, *SIMKK-RNAi* and GFP-SIMK lines, originating from somatic embryos, were inoculated with *S. meliloti* wild-type. Inoculated plants were daily subjected to microscopic observations, ITs were counted,

563 and evaluation of ITs number per the whole root system length was performed at 10 dpi with
564 *S. meliloti* using Axio Zoom.V16 Stereo microscope (Carl Zeiss, Germany).

565 *Image acquisition and processing*

566 The image acquisition, post-processing, semi-quantitative profile measurements, quantitative
567 colocalization analysis, maximum intensity projections from individual z-stacks, subset
568 creation of all fluorescence images, and 3D modeling was made using Zeiss ZEN software
569 (Black and Blue versions, Carl Zeiss, Germany). Data obtained by LSFM imaging were
570 subjected to 3D rendering. A subset of selected z-stacks was created from the whole root
571 volume to capture different stages of root nodulation. Data were imported to Arivis Vision4D
572 2.12.6 software (Arivis AG, Rostock, Germany), automatically converted to a *.sis file,
573 displayed as 3D objects, and rendered in the maximum intensity mode. Animations and
574 videos were prepared by clipping 3D models in XZ and YZ planes and by using rotation and
575 zooming tools in the 4D clipping panel by arranging keyframes. Although quantification of
576 fluorescence intensities is not influenced by post-acquisition look-up table (LUT) intensity
577 adjustments, all images used for semi-quantitative and quantitative analyses were acquired at
578 the same imaging conditions. The same laser attenuation values for all laser lines were set
579 prior to the acquisition and the thickness of individual optical sections was optimized
580 according to Nyquist criteria. The pinhole sizes for green (GFP), red (Alexa Fluor 555) and
581 yellow (Alexa Fluor 647) channels were matched and the range of detection was appropriately
582 adjusted to ensure separation of emission wavelengths and to prevent fluorescence spectral
583 bleed-through. The brightness and contrast of all acquired images were uniformly adjusted
584 and images exported from ZEN software were assembled into final figure plates using
585 Microsoft PowerPoint.

586 *Semi-quantitative analysis of the fluorescence intensity distribution*

587 Data obtained from LSFM imaging were semi-quantitatively evaluated by profile
588 measurements to study the fluorescence intensity distribution of GFP-tagged SIMK in alfalfa
589 root hairs and its association with *S. meliloti* at early symbiotic stages. GFP-SIMK mean
590 fluorescence intensity was quantitatively evaluated in specific regions of interest (ROIs)
591 inside root hairs growing under control conditions or interacting with rhizobia. Distribution of
592 SIMK, GFP and activated MAPKs around early invasion structures was determined on fixed
593 and immunolabeled samples inside root hairs of alfalfa control and transgenic plants by semi-

quantitative analysis and profile measurement of fluorescence intensities. Intensity profiles were quantified across infection pockets and ITs as indicated in appropriate images. These analyses were done using a profile or measure function of Zeiss ZEN 2011 software (Black version) from single confocal optical sections or maximum intensity projections.

Quantitative colocalization analysis

The mode of fluorescence signals colocalization was analyzed on immunolabeled root samples of alfalfa control and transgenic plants co-cultivated with *S. meliloti*. Quantitative colocalization analysis between SIMK and activated MAPKs was conducted in particular ROIs at early symbiotic stages around infection pockets and ITs. The colocalization range was measured from single plane confocal sections, and in total, three independent optical sections per infection pocket and IT were analyzed using the colocalization tool of Zeiss ZEN 2014 software (Blue version). Background thresholds were automatically implemented by the iterative Costes approach (Costes *et al.*, 2004) and colocalization data were calculated from manually selected ROIs. Data were displayed in intensity-corrected scatterplot diagrams, the intensity correlation of colocalizing pixels was expressed by Pearson's correlative coefficient and results were graphically edited using Microsoft Excel.

Statistical analysis

Statistical parameters of performed experiments, number of samples (N), type of statistical test and statistical significance represented by asterisks are included in the figure legends. The statistical significance of differences between treatments was calculated in Microsoft Excel using a t-test and it is indicated by asterisks (* $p < 0.05$, ** $p < 0.01$, *** $p < 0.001$, n.s. no statistical significance).

Supplemental Data

Supplemental Figure S1. Quantitative colocalization analysis of MAPKs around infection pockets in root hairs of control and transgenic plants during an early stage of *M. sativa – S. meliloti* symbiotic interaction.

Supplemental Figure S2. Quantitative colocalization analysis of MAPKs around ITs in root hairs of control and transgenic plants during *M. sativa – S. meliloti* symbiotic interaction.

622 **Supplemental Figure S3.** Effectivity of ITs formation in control and transgenic plants after
623 inoculation with *S. meliloti*.

624 **Supplemental Movie S1.** 3D volumetric root rendering of GFP-SIMK line symbiotically
625 interacting with *S. meliloti* expressing mRFP.

626 **Supplemental Movie S2.** Orthogonal projection of the root hair showing GFP-SIMK
627 association with rhizobia at the docking site from a X-Z view.

628 **Supplemental Movie S3.** Orthogonal projection of the root hair showing GFP-SIMK
629 association with rhizobia at the docking site from a Y-Z view.

630 **Supplemental Movie S4.** Orthogonal projection of the root hair showing GFP-SIMK
631 association with a cluster of rhizobia located at the infection site in the neck of root hair curl
632 from a X-Z view.

633 **Supplemental Movie S5.** Orthogonal projection of the root hair showing GFP-SIMK
634 association with a cluster of rhizobia located at the infection site in the neck of root hair curl
635 from a Y-Z view.

636 **Supplemental Movie S6.** Orthogonal projection of the root hair showing a very tight
637 association of GFP-SIMK with rhizobia at the infection site before rhizobia entry from a X-Z
638 view.

639 **Supplemental Movie S7.** Orthogonal projection of the root hair showing a very tight
640 association of GFP-SIMK with rhizobia at the infection site before rhizobia entry from a Y-Z
641 view.

642 **Supplemental Movie S8.** Orthogonal projection of the root hair showing association of GFP-
643 SIMK with rhizobia entrapped inside root hair curl at the beginning of infection pocket
644 formation from a X-Z view.

645 **Supplemental Movie S9.** Orthogonal projection of the root hair showing association of GFP-
646 SIMK with rhizobia entrapped inside root hair curl at the beginning of infection pocket
647 formation from a Y-Z view.

Supplemental Movie S10. Orthogonal projection of the root hair showing association of GFP-SIMK with rhizobia forming colonies within infection pocket at the beginning of IT formation from a X-Z view.

Supplemental Movie S11. Orthogonal projection of the root hair showing association of GFP-SIMK with rhizobia forming colonies within infection pocket at the beginning of IT formation from a Y-Z view.

Supplemental Movie S12. Time-lapse imaging of GFP-SIMK accumulation in the nucleus and at the infection site in the root hair during rhizobia attachment.

Supplemental Movie S13. Time-lapse imaging of GFP-SIMK accumulation around infection pockets in the root hair.

Supplemental Movie S14. Time-lapse imaging of GFP-SIMK accumulation in the nucleus and at the infection site in the root hair during rhizobia attachment analyzed by semi-quantitative GFP-SIMK fluorescence intensity distribution.

Supplemental Movie S15. Time-lapse imaging of GFP-SIMK accumulation around infection pockets in the root hair analyzed by semi-quantitative GFP-SIMK fluorescence intensity distribution.

Funding

This work was funded by ERDF project Plants as a tool for sustainable global development (CZ.02.1.01/0.0/0.0/16_019/0000827).

Acknowledgment

We would like to thank Katarína Takáčová and Monika Vadovičová for their technical help in all stages of the presented work and Dr. Pavlína Mikulková for her expert technical help with LSFM imaging.

Authors' contributions

KH, OŠ and MH conducted immunolocalization experiments, KH, MO and OŠ conducted CLSM, ACLSM and LSFM microscopic documentation, KH performed the quantitative evaluation and statistical analyses. MH prepared and selected transgenic alfalfa lines. JŠ and MO contributed to the experimental plan and data interpretation. KH and MO wrote the manuscript with input from all co-authors. JŠ provided infrastructure and secured funding.

Conflicts of interest

The authors declare that they have no conflict of interest.

Data Availability

Data that support the findings of this study are available from the corresponding author upon reasonable request.

Figure legends

Figure 1. Subcellular immunolocalization of SIMK and activated MAPKs in growing root hairs of alfalfa control and transgenic plants under control conditions. (A-J) Whole-mount immunofluorescence localization of SIMK and activated MAPKs in root hairs of alfalfa RSY plants **(A-C)** and plants of transgenic *SIMKK-RNAi* **(D-F)** and GFP-SIMK **(G-J)** lines. SIMK (in magenta) was immunostained with SIMK-specific antibody **(A,D,G)** and activated MAPKs (pERK, in yellow) using phospho-specific pERK 44/42 antibody **(B,E,H)**. Overlay of bright-field images with fluorescence channels **(C,F,I)**, GFP-tagged SIMK (in green) was localized via GFP fluorescence in fixed root hair of transgenic GFP-SIMK line **(J)**. **(K,M,O)** Fluorescence intensity profiles of SIMK, activated MAPKs, and GFP-tagged SIMK distribution along the measured line shown in **(L,N,P)**. Scale bar = 5 μm **(A-J; L,N,P)**.

Figure 2. Live cell imaging of early nodulation stages in roots of transgenic GFP-SIMK line at 3 dpi with mRFP-labeled *S. meliloti* using LSFM. (A) 3D rendering overview of alfalfa root stably expressing GFP-tagged SIMK (green) co-cultivated with mRFP-labeled rhizobia (magenta). Rhizobia growing on the surface of agar plates are associated with a portion of the root and root hairs that were in contact with the agar plate surface. **(B)** Position of nuclei in root hairs not interacting with rhizobia (arrows). **(C)** Position of nuclei in root hairs interacting with rhizobia (arrows). **(D-F)** Details of root hair infection during rhizobia attachment and internalization (arrowheads). Scale bar = 20 μm **(D-F)**, 40 μm **(B-C)**.

Figure 3. Quantitative analysis of GFP-SIMK fluorescence intensity distribution in nuclei and tips of alfalfa root hairs under control conditions and upon symbiotic interaction with mRFP-labeled *S. meliloti*. (A-B) GFP-SIMK distribution in non-interacting root hairs **(A)** and root hairs symbiotically interacting with rhizobia **(B)**. Measurement of GFP-SIMK mean fluorescence intensity was performed in nuclei and root hair tips of non-

interacting root hairs **(A**, marked by white dashed boxes**)** and in nuclei and infection sites of interacting root hairs **(B**, marked by white dashed boxes**)**. **(C-E)** Quantitative evaluation of GFP-SIMK signal intensity in non-interacting root hairs **(C,** N=6**)** and in interacting root hairs **(D,** N=6**)**, and comparison of GFP-SIMK signal intensity in nuclei of non-interacting and interacting root hairs **(E,** N=6**)**. Statistical differences were calculated in Microsoft Excel using t-test. Error bars show ± standard deviation (SD). Asterisks indicate statistical significance between treatments (*p < 0,05, **p < 0,01, ***p < 0.001). Scale bar = 20 µm **(A-B)**.

Figure 4. Live cell localization of GFP-SIMK and its association with mRFP-labeled *S. meliloti* during early nodulation stages in root hairs 3 to 4 dpi using LSFM. (A-E) Selected root hairs at early sequential infection stages showing the distribution of GFP-SIMK (green) and rhizobia (magenta) during attachment to the root hairs **(A)**, followed by rhizobia internalization **(B, C)**, infection pocket formation **(D)**, and rhizobia enclosure inside infection pockets **(E)**. **(F-Y)** Detailed qualitative and semi-quantitative analysis of GFP-SIMK (green) and rhizobia (magenta) distribution during attachment to the root hairs **(F-I),** rhizobia internalization **(J-Q)**, infection pocket formation **(R-U)**, and rhizobia enclosure inside infection pockets **(V-Y)**. Semi-quantitative evaluation of GFP-SIMK and mRFP-labeled rhizobia fluorescence distribution **(G,K,O,S,W)** along dashed arrows in **(F,J,N,R,V)**, indicating GFP-SIMK distribution in symbiotically infected root hairs (grey dashed arrows) and its association with rhizobia at specific infection sites (yellow dashed arrows). Representative images prepared from orthogonal projections in X-Z views **(H,L,P,T,X)** and Y-Z views **(I,M,Q,U,Y)** show a detailed view of GFP-SIMK accumulation around fluorescently labeled rhizobia (marked with a white dashed boxes). Black arrows in **(G,K,O,S,W)** show increased accumulation of GFP-SIMK. Green dots in **(C,N)** are fiducial markers. Scale bar = 10 µm **(F,J,N,R,V)**.

Figure 5. Subcellular immunolocalization of SIMK and activated MAPKs around infection pockets in curled root hairs after inoculation with *S. meliloti*. (A,E,I) Localization of DAPI-stained rhizobia inside infection pocket of RSY **(A)**, *SIMKK-RNAi* **(E)**, and GFP-SIMK **(I)** lines. **(B,F,J)** SIMK immunostained with SIMK-specific antibody and overlaid with DAPI in RSY **(B)**, *SIMKK-RNAi* **(F)**, and GFP-SIMK **(J)** lines. **(C,G,K)** Activated MAPKs immunostained with phospho-specific pERK 44/42 antibody and overlaid with DAPI in RSY **(C)**, *SIMKK-RNAi* **(G)**, and GFP-SIMK **(K)** lines. **(D,H,L)** Overlay of DAPI, SIMK and activated MAPKs in RSY **(D)**, *SIMKK-RNAi* **(H)**, and GFP-SIMK **(L)** lines. **(M,N)** GFP-tagged SIMK overlaid with DAPI **(M)** and overlay of GFP-tagged SIMK, SIMK immunostained with SIMK-specific antibody and DAPI in transgenic GFP-SIMK line **(N)**. **(O,P,Q,R)** The fluorescence intensity distribution of SIMK, activated MAPKs, GFP-tagged SIMK, and DAPI was measured along profiles indicated by white dashed arrows in **(D,H,L,N)**. Black arrows indicate the plasma membrane of the infection pocket, black arrowheads indicate the root hair plasma membrane. Scale bar = 5 µm **(A-N)**.

Figure 6. Quantitative analysis of SIMK and phosphorylated MAPKs fluorescence intensity distribution around infection pockets in curled root hairs after inoculation with *S. meliloti*. (A-F) Immunolocalization of SIMK **(A-C)** and phosphorylated MAPKs **(D-F)** in

infection pockets of RSY **(A,D**; N=10 for SIMK, N=7 for pERK**)**, *SIMKK-RNAi* **(B,E**; N=10 for SIMK, N=7 for pERK**)**, and GFP-SIMK **(C,F**; N=9 for SIMK, N=7 for pERK**)**. White dashed lines in **(A-F)** indicate defined ROIs in which the mean fluorescence intensity was measured. **(G,H)** Quantitative evaluation of SIMK **(G)** and activated MAPKs **(H)** signal intensity in transgenic *SIMKK-RNAi* and GFP-SIMK lines compared to RSY plants. Statistical differences were calculated in Microsoft Excel using t-test. Error bars show ± standard deviation (SD). Asterisks indicate statistical significance between treatments (**p < 0,01, ***p < 0.001, n.s. no statistical significance). Scale bar = 2 µm **(A-F)**.

Figure 7. Subcellular immunolocalization of SIMK and activated MAPKs around ITs in root hairs induced after inoculation with *S. meliloti*. **(A,E,I)** Localization of DAPI-stained rhizobia inside ITs of RSY **(A)**, *SIMKK-RNAi* **(E)**, and GFP-SIMK **(I)** lines. **(B,F,J)** SIMK immunostained with SIMK-specific antibody and overlaid with DAPI in RSY **(B)**, *SIMKK-RNAi* **(F)**, and GFP-SIMK **(J)** lines. **(C,G,K)** Activated MAPKs immunostained with phospho-specific pERK 44/42 antibody and overlaid with DAPI in RSY **(C)**, *SIMKK-RNAi* **(G)**, and GFP-SIMK **(K)** lines. **(D,H,L)** Overlay of DAPI, SIMK and activated MAPKs in RSY **(D)**, *SIMKK-RNAi* **(H)**, and GFP-SIMK **(L)** plants. **(M,N)** GFP-tagged SIMK overlaid with DAPI **(M)** and overlay of GFP-tagged SIMK, SIMK immunostained with SIMK-specific antibody and DAPI in transgenic GFP-SIMK line **(N)**. **(O,P,Q,R)** The fluorescence intensity distribution of SIMK, activated MAPKs, GFP-tagged SIMK, and DAPI was measured along profiles indicated by white dashed arrows in **(D,H,L,N)**. Black arrows indicate the plasma membrane of IT, black arrowheads indicate the plasma membrane of root hair. Scale bar = 5 µm **(A-N)**.

Figure 8. Quantitative analysis of SIMK and phosphorylated MAPKs fluorescence intensity distribution around ITs in root hairs after inoculation with *S. meliloti*. **(A-F)** Immunolocalization of SIMK **(A-C)** and phosphorylated MAPKs **(D-F)** in ITs of RSY **(A,D**; N=8 for SIMK, N=8 for pERK**)**, *SIMKK-RNAi* **(B,E**; N=6 for SIMK, N=7 for pERK**)**, and GFP-SIMK **(C,F**; N=8 for SIMK, N=8 for pERK**)**. White dashed lines in **(A-F)** indicate defined ROIs in which the mean fluorescence intensity was measured. **(G,H)** Quantitative evaluation of SIMK **(G)** and activated MAPKs **(H)** signal intensity in transgenic *SIMKK-RNAi* and GFP-SIMK lines compared to RSY plants. Statistical differences were calculated in Microsoft Excel using t-test. Error bars show ± standard deviation (SD). Asterisks indicate statistical significance between treatments (*p < 0,05, ***p < 0.001, n.s. no statistical significance). Scale bar = 5 µm **(A-F)**.

Figure 9. Volume 3D rendering of rhizobia-containing early symbiotic structures with immunolabeled SIMK and membranes visualized using FM4-64FX in root hairs after inoculation with *S. meliloti*. **(A-D)** RSY root hairs. **(E-H)** Root hairs of *SIMKK-RNAi* line. **(I-L)** Root hairs of GFP-SIMK line. Subcellular localization of SIMK with membranes of infection pockets **(A,C,E,G,I,K)** and ITs **(B,D,F,HJ,L)**. Overlay of membranes (in magenta), SIMK (in green) and DAPI-stained rhizobia (in blue). **(M)** Averaged Pearson‘s correlative coefficients of colocalization analysis between SIMK and FM4-64FX-stained membranes around infection pockets and ITs. Details of infection pockets and ITs shown in **(C, D, G, H, K, L)** are marked with a white dashed boxes in **(A,B,E,F,I,J)**.

790

791 **References:**

792 **Bekešová S, Komis G, Křenek P, Vyplelová P, Ovečka M, Luptovčiak I, Šamaj J** (2015)
793 Monitoring protein phosphorylation by acrylamide pendant Phos-Tag^{TM} in various plants.
794 Front Plant Sci **6**: 336

795 **Bisseling T, Geurts R** (2020) Specificity in legume nodule symbiosis. Science **369**: 620–621

796 **Brewin NJ** (2004) Plant cell wall remodeling in the rhizobium-legume symbiosis. Crit Rev
797 Plant Sci **23**: 293–316

798 **Brundrett MC** (2002) Coevolution of roots and mycorrhizas of land plants. New Phytol **154**:
799 275–304

800 **Cardinale F, Jonak C, Ligterink W, Niehaus K, Boller T, Hirt H** (2000) Differential
801 activation of four specific MAPK pathways by distinct elicitors. J Biol Chem **275**: 36734–
802 36740

803 **Cardinale F, Meskiene I, Ouaked F, Hirt H** (2002) Convergence and divergence of stress-
804 induced mitogen-activated protein kinase signaling pathways at the level of two distinct
805 mitogen-activated protein kinase kinases. Plant Cell **14**: 703–711

806 **Checcucci A, Azzarello E, Bazzicalupo M, Galardini M, Lagomarsino A, Mancuso S,**
807 **Marti L, Marzano MC, Mocali S, Squartini A, Zanardo M, Mengoni A** (2016) Mixed
808 Nodule Infection in *Sinorhizobium meliloti-Medicago sativa* Symbiosis Suggest the Presence
809 of Cheating Behavior. Front Plant Sci **7**: 835

810 **Chen T, Zhou B, Duan L, Zhu H, Zhang Z** (2017) MtMAPKK4 is an essential gene for
811 growth and reproduction of *Medicago truncatula*. Physiol Plant **159**: 492–503

812 **Chen T, Zhu H, Ke D, Cai K, Wang C, Gou H, Hong Z, Zhang Z** (2012) A MAP kinase
813 kinase interacts with SymRK and regulates nodule organogenesis in *Lotus japonicus*. Plant
814 Cell **24**: 823–838

815 **Clúa J, Roda C, Zanetti ME, Blanco FA** (2018) Compatibility between Legumes and
816 Rhizobia for the Establishment of a Successful Nitrogen-Fixing Symbiosis. Genes (Basel) **9**:
817 125

818 **Costes SV, Daelemans D, Cho EH, Dobbin Z, Pavlakis G, Lockett S** (2004) Automatic
819 and quantitative measurement of protein-protein colocalization in live cells. Biophys J **86**:
820 3993–4003

821 **Dénarié J, Cullimore J** (1993) Lipo-oligosaccharide nodulation factors: A new class of
822 signaling molecules mediating recognition and morphogenesis. Cell **74**: 951–954

823 **Fåhreus G** (1957) The infection of clover root hairs by nodule bacteria studied by a simple
824 glass slide technique. J Gen Microbiol **16**: 374–381

Fournier J, Teillet A, Chabaud M, Ivanov S, Genre A, Limpens E, de Carvalho-Niebel F, Barker DG (2015) Remodelling of the infection chamber before infection thread formation reveals a two-step mechanism for rhizobial entry into the host legume root hair. *Plant Physiol* **167**: 1233–1242

Fournier J, Timmers AC, Sieberer BJ, Jauneau A, Chabaud M, Barker DG (2008) Mechanism of infection thread elongation in root hairs of *Medicago truncatula* and dynamic interplay with associated rhizobial colonization. Plant Physiol **148**: 1985–1995

Gage DJ (2004) Infection and Invasion of Roots by Symbiotic, Nitrogen-Fixing Rhizobia during Nodulation of Temperate Legumes. Microbiol Mol Biol Rev **68**: 280–300

Grimsrud PA, den Os D, Wenger CD, Swaney DL, Schwartz D, Sussman MR, Ané JM, Coon JJ (2010) Large-scale phosphoprotein analysis in *Medicago truncatula* roots provides insight into *in vivo* kinase activity in legumes. Plant Physiol **152**: 19–28

Hrbáčková M, Luptovčiak I, Hlaváčková K, Dvořák P, Tichá M, Šamajová O, Novák D, Bednarz H, Niehaus K, Ovečka M, Šamaj J (2021) Overexpression of alfalfa SIMK promotes root hair growth, nodule clustering and shoot biomass production. Plant Biotechnol J **19**: 767–784

Ibáñez F, Wall L, Fabra A (2017) Starting points in plant-bacteria nitrogen-fixing symbioses: intercellular invasion of the roots. J Exp Bot **68**: 1905–1918

Jones KM, Kobayashi H, Davies BW, Taga, ME, Walker, GC (2007) How rhizobial symbionts invade plants: the *Sinorhizobium* - *Medicago* model. Nat Rev Microbiol **5**: 619–633

Kidaj D, Krysa M, Susniak K, Matys J, Komaniecka I, Sroka-Bartnicka A (2020) Biological activity of Nod factors. Acta Biochim Pol **67**: 435–440

Kiegerl S, Cardinale F, Siligan C, Gross A, Baudouin E, Liwosz A (2000) SIMKK, a mitogen-activated protein kinase (MAPK) kinase, is a specific activator of the salt stress-induced MAPK, SIMK. Plant Cell **12**: 2247–2258

Komis G, Šamajová O, Ovečka M, Šamaj J (2018) Cell and Developmental Biology of Plant Mitogen-Activated Protein Kinases. Annu Rev Plant Biol **69**: 237–265

Lopez-Gomez M, Sandal N, Stougaard J, Boller T (2012) Interplay of flg22-induced defence responses and nodulation in *Lotus japonicus*. J Exp Bot **63**: 393–401

Munnik T, Ligterink W, Meskiene I, Calderini O, Beyerly J, Musgrave A, Hirt H (1999) Distinct osmo-sensing protein kinase pathways are involved in signalling moderate and severe hyper-osmotic stress. Plant J **20**: 381–388

Oldroyd GED (2013) Speak, friend, and enter: signalling systems that promote beneficial symbiotic associations in plants. *Nat Rev Microbiol* **11**: 252–263

Oldroyd GED, Downie JA (2008) Coordinating nodule morphogenesis with rhizobial infection in legumes. Annu Rev Plant Biol **59**: 519–46

Oldroyd GED, Murray JD, Poole PS, Downie JA (2011) The Rules of Engagement in the Legume-Rhizobial Symbiosis. *Annu Rev Genet* **45**: 119–144

Ovečka M, Takáč T, Komis G, Vadovič P, Bekešová S, Doskočilová A, Smékalová V, Luptovčiak I, Šamajová O, Schweighofer A, Meskiene I, Jonak C, Křenek P, Lichtscheidl I, Škultéty Ľ, Hirt H, Šamaj J (2014) Salt-induced subcellular kinase relocation and seedling susceptibility caused by overexpression of *Medicago* SIMKK in *Arabidopsis.* J Exp Bot **65**: 2335–2350

Ovečka M, Vaškebová L, Komis G, Luptovčiak I, Smertenko A, Šamaj J (2015) Preparation of plants for developmental and cellular imaging by lightsheet microscopy. Nat Protoc **10**: 1234–1247

Ovečka M, **von Wangenheim D, Tomančák P, Šamajová O, Komis G, Šamaj J** (2018) Multiscale imaging of plant development by light-sheet fluorescence microscopy. Nat Plants **4**: 639–650

Ovečka M, Sojka J, Tichá M, Komis G, Basheer J, Marchetti C, Šamajová O, Kuběnová L, Šamaj J (2022) Imaging plant cells and organs with light-sheet and super-resolution microscopy. Plant Physiol **188**: 683–702

Pitzschke A (2015) Modes of MAPK substrate recognition and control. Trends Plant Sci **20**: 49–55

Poole P, Ramachandran V, Terpolilli J (2018) Rhizobia: from saprophytes to endosymbionts. Nat Rev Microbiol **16**: 291–303

Radović J, Sokolović D, Marković J (2009) Alfalfa-most important perennial forage legume in animal husbandry. Biotechnol Anim Husb **25**: 465–475

Rae AE, Rolland V, White RG, Mathesius U (2021) New methods for confocal imaging of infection threads in crop and model legumes. Plant Methods **17**: 24

Rashid MH, Krehenbrink M, Akhtar MS (2015) Nitrogen-Fixing Plant-Microbe Symbioses. In: *Sustainable Agriculture Reviews* (Lichtfouse, E., eds.), Springer International Publishing Switzerland **15**: 193–234

Rasmussen MW, Roux M, Petersen M, Mundy J (2012) MAP kinase cascades in *Arabidopsis* innate immunity. *Front Plant Sci* **3**: 169

Roy S, Liu W, Nandety RS, Crook A, Mysore KS, Pislariu CI, Frugoli J, Dickstein R, Udvardi MK (2020) Celebrating 20 years of genetic discoveries in legume nodulation and symbiotic nitrogen fixation. Plant Cell **32**: 15–41

Ryu H, Laffont C, Frugier F, Hwang I (2017) MAP Kinase-Mediated Negative Regulation of Symbiotic Nodule Formation in *Medicago truncatula*. *Mol Cells* **40**: 17–23

Samac DA, Austin-Phillips S (2006) Alfalfa (*Medicago sativa* L.). In: *Agrobacterium Protocols*. *Methods Mol Biol.* (Wang, K., ed.) Clifton, N. J.: Humana Press, 301–312

Šamaj J, Ovečka M, Hlavacka A, Lecourieux F, Meskiene I, Lichtscheidl I, Lenart P, Salaj J, Volkmann D, Bögre L, Baluska F, Hirt H (2003) Involvement of MAP kinase SIMK and actin cytoskeleton in the regulation of root hair tip growth. Cell Biol Int **27**: 257–259

Šamaj J, Ovečka M, Hlavacka A, Lecourieux F, Meskiene I, Lichtscheidl I, Lenart P, Salaj J, Volkmann D, Bögre L, Baluška F, Hirt H (2002) Involvement of the mitogen-activated protein kinase SIMK in regulation of root hair tip growth. *EMBO J* **21**: 3296–2306

Šamajová O, Plíhal O, Al-Yousif M, Hirt H, Šamaj J (2013) Improvement of stress tolerance in plants by genetic manipulation of mitogen-activated protein kinases. Biotechnol Adv **31**: 118–128

Shaw SL, Long SR (2003) Nod factor inhibition of reactive oxygen efflux in a host legume. Plant Physiol **132**: 2196–2204

Smékalová V, Doskočilová A, Komis G, Šamaj J (2014) Crosstalk between secondary messengers, hormones and MAPK modules during abiotic stress signalling in plants. Biotechnol Adv **32**: 2–11

Sprent JI (2008) 60Ma of legume nodulation. What's new? What's changing? J Exp Bot **59**: 1081–1084

Sprent JI, James E (2007) Legume evolution: Where do nodules and mycorrhizas fit in? Plant Physiol **144**: 575–581

Sun T, Zhang Y (2022) MAP kinase cascades in plant development and immune signaling. EMBO Rep **23**: e53817

Terpolilli JJ, Hood GA, Poole PS (2012) What determines the efficiency of N_2-fixing *Rhizobium*-Legume Symbioses. Adv Microb Physiol **60**: 325–389

Tichá M, Hlaváčková K, Hrbáčková M, Ovečka M, Šamajová O, Šamaj J (2020) Super-resolution imaging of microtubules in *Medicago sativa*. Methods Cell Biol **160**: 237–251

Timmers ACJ (2008) The role of the plant cytoskeleton in the interaction between legumes and rhizobia. J Microsc **231**: 247–256

Vyplelová P, Ovečka M, Komis G, Šamaj J (2018) Advanced microscopy methods for bioimaging of mitotic microtubules in plants. Methods in Cell Biology **145**: 129–158

Walker L, Lagunas D, Gifford ML (2020) Determinants of Host Range Specifity in Legume-Rhizobia Symbiosis. Front Microbiol **11**: 585749

Wang Q, Liu J, Zhu H (2018) Genetic and molecular mechanisms underlying symbiotic specificity in legume-rhizobium interactions. Front Plant Sci **9**: 313

White J, Prell J, James EK, Poole P (2007) Nutrient sharing between symbionts. Plant Physiol **144**: 604–614

Xu J, Zhang S (2015) Mitogen-activated protein kinase cascades in signaling plant growth and development. Trends Plant Sci **20**: 56–64

Yan Z, Cao J, Fan Q, Chao H, Guan X, Zhang Z, Duanmu D (2020) Dephosphorylation of LjMPK6 by phosphatase LjPP2C is involved in regulating nodule organogenesis in *Lotus japonicus*. Int J Mol Sci **21**: 5565.

Yang J, Lan L, Jin Y, Yu N, Wang D, Wang E (2022) Mechanisms underlying legume-rhizobium symbioses. J Integr Plant Biol **64**: 244–267

Yin J, Guan X, Zhang H, Wang L, Li H, Zhang Q, Chen T, Zeyuan X, Hong Z, Cao Y, Zhang Z (2019) An MAP kinase interacts with LHK1 and regulates nodule organogenesis in *Lotus japonicus*. Sci China Life Sci **62**: 1203–1217

Zhang M, Zhang S (2022) Mitogen-activated protein kinase cascades in plant signaling. J Integr Plant Biol **64**: 301– 341

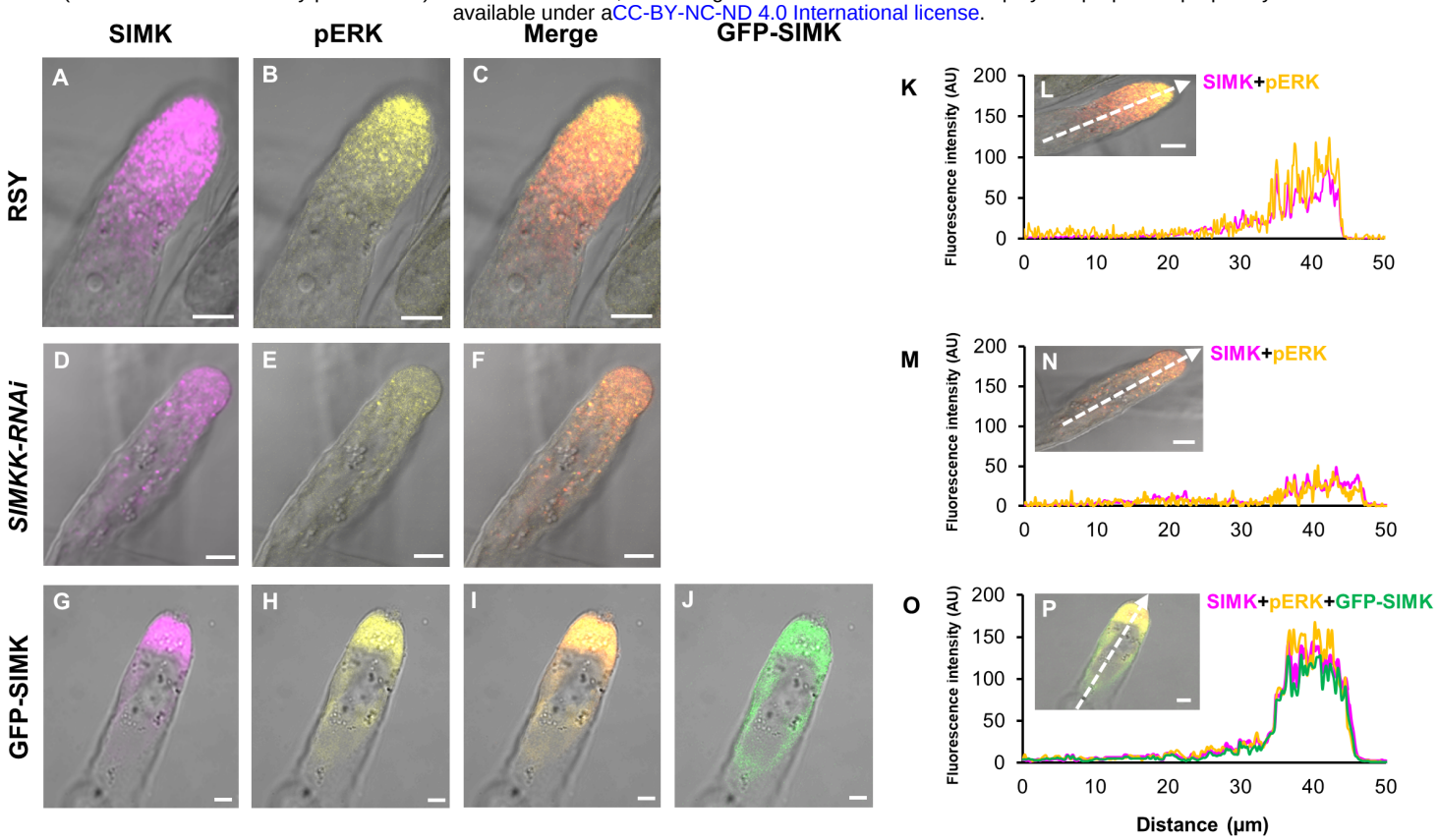

Figure 1. Subcellular immunolocalization of SIMK and activated MAPKs in growing root hairs of alfalfa control and transgenic plants under control conditions. (A-J) Whole-mount immunofluorescence localization of SIMK and activated MAPKs in root hairs of alfalfa RSY plants **(A-C)** and plants of transgenic *SIMKK-RNAi* **(D-F)** and GFP-SIMK **(G-J)** lines. SIMK (in magenta) was immunostained with SIMK-specific antibody **(A,D,G)** and activated MAPKs (pERK, in yellow) using phospho-specific pERK 44/42 antibody **(B,E,H)**. Overlay of bright-field images with fluorescence channels **(C,F,I)**, GFP-tagged SIMK (in green) was localized via GFP fluorescence in fixed root hair of transgenic GFP-SIMK line **(J)**. **(K,M,O)** Fluorescence intensity profiles of SIMK, activated MAPKs, and GFP-tagged SIMK distribution along the measured line shown in **(L,N,P)**. Scale bar = 5 μm **(A-J; L,N,P)**.

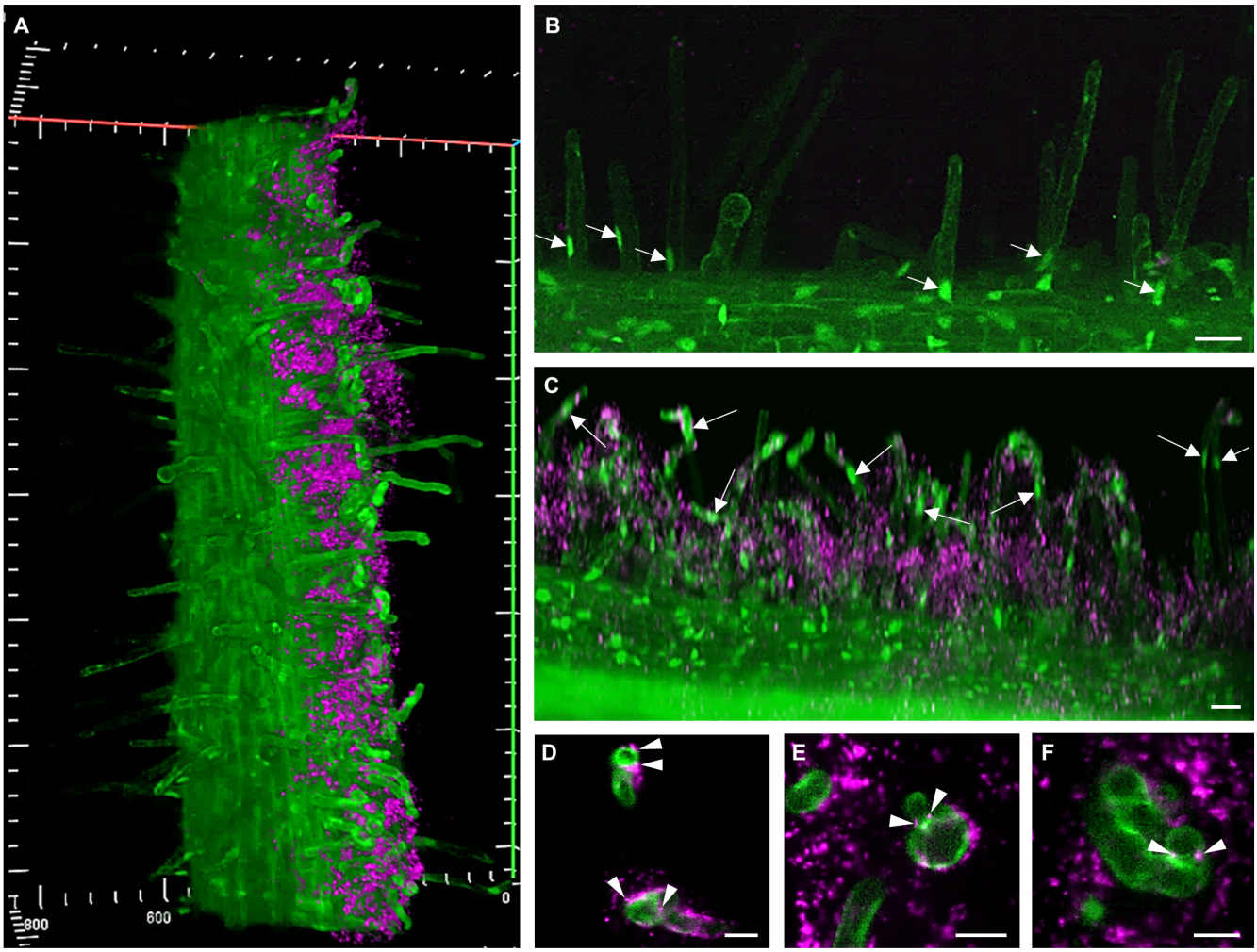

Figure 2. Live cell imaging of early nodulation stages in roots of transgenic GFP-SIMK line at 3 dpi with mRFP-labeled *S. meliloti* using LSFM. (A) 3D rendering overview of alfalfa root stably expressing GFP-tagged SIMK (green) co-cultivated with mRFP-labeled rhizobia (magenta). Rhizobia growing on the surface of agar plates are associated with a portion of the root and root hairs that were in contact with the agar plate surface. **(B)** Position of nuclei in root hairs not interacting with rhizobia (arrows). **(C)** Position of nuclei in root hairs interacting with rhizobia (arrows). **(D-F)** Details of root hairs infection during rhizobia attachment and internalization (arrowheads). Scale bar = 20 µm **(D-F)**, 40 µm **(B-C)**.

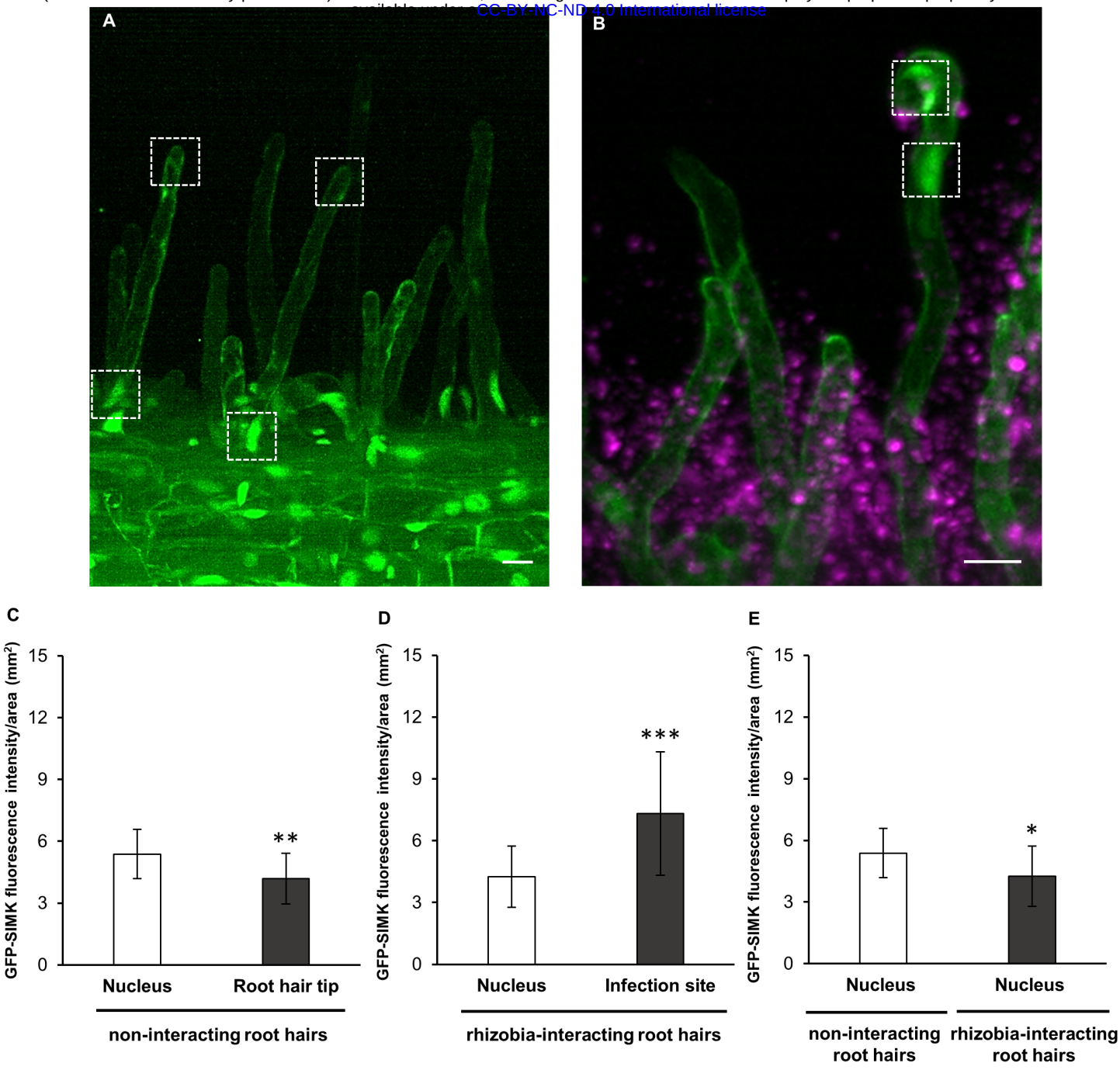

Figure 3. Quantitative analysis of GFP-SIMK fluorescence intensity distribution in nuclei and tips of alfalfa root hairs under control conditions and upon symbiotic interaction with mRFP-labeled *S. meliloti*. (A-B) GFP-SIMK distribution in non-interacting root hairs **(A)** and root hairs symbiotically interacting with rhizobia **(B)**. Measurement of GFP-SIMK mean fluorescence intensity was performed in nuclei and root hair tips of non-interacting root hairs **(A**, marked by white dashed boxes**)** and in nuclei and infection sites of interacting root hairs **(B**, marked by white dashed boxes**)**. **(C-E)** Quantitative evaluation of GFP-SIMK signal intensity in non-interacting root hairs **(C,** N=6**)** and in interacting root hairs **(D,** N=6**)**, and comparison of GFP-SIMK signal intensity in nuclei of non-interacting and interacting root hairs **(E,** N=6**)**. Statistical differences were calculated in Microsoft Excel using t-test. Error bars show ± standard deviation (SD). Asterisks indicate statistical significance between treatments (*p < 0,05, **p < 0,01, ***p < 0.001). Scale bar = 20 μm **(A-B)**.

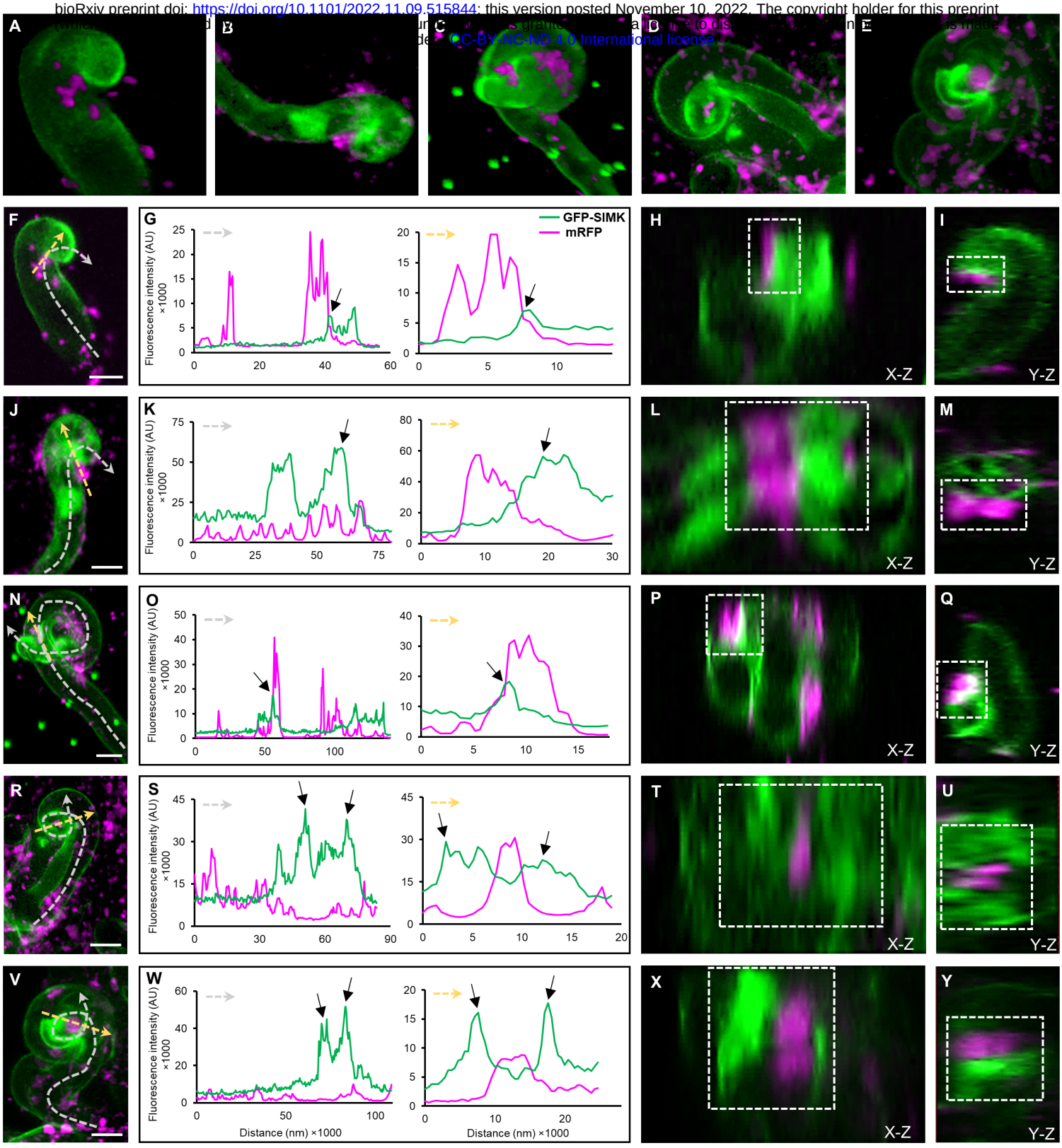

Figure 4. Live cell localization of GFP-SIMK and its association with mRFP-labeled *S. meliloti* during early nodulation stages in root hairs 3 to 4 dpi using LSFM. (A-E) Selected root hairs at early sequential infection stages showing the distribution of GFP-SIMK (green) and rhizobia (magenta) during attachment to the root hairs **(A)**, followed by rhizobia internalization **(B, C)**, infection pocket formation **(D)**, and rhizobia enclosure inside infection pockets **(E)**. **(F-Y)** Detailed qualitative and semi-quantitative analysis of GFP-SIMK (green) and rhizobia (magenta) distribution during attachment to the root hairs **(F-I),** rhizobia internalization **(J-Q)**, infection pocket formation **(R-U)**, and rhizobia enclosure inside infection pockets **(V-Y)**. Semi-quantitative evaluation of GFP-SIMK and mRFP-labeled rhizobia fluorescence distribution **(G,K,O,S,W)** along dashed arrows in **(F,J,N,R,V)**, indicating GFP-SIMK distribution in symbiotically infected root hairs (grey dashed arrows) and its association with rhizobia at specific infection sites (yellow dashed arrows). Representative images prepared from orthogonal projections in X-Z views **(H,L,P,T,X)** and Y-Z views **(I,M,Q,U,Y)** show a detailed view of GFP-SIMK accumulation around fluorescently labeled rhizobia (marked with a white dashed boxes). Black arrows in **(G,K,O,S,W)** show increased accumulation of GFP-SIMK. Green dots in **(C,N)** are fiducial markers. Scale bar = 10 µm **(F,J,N,R,V)**.

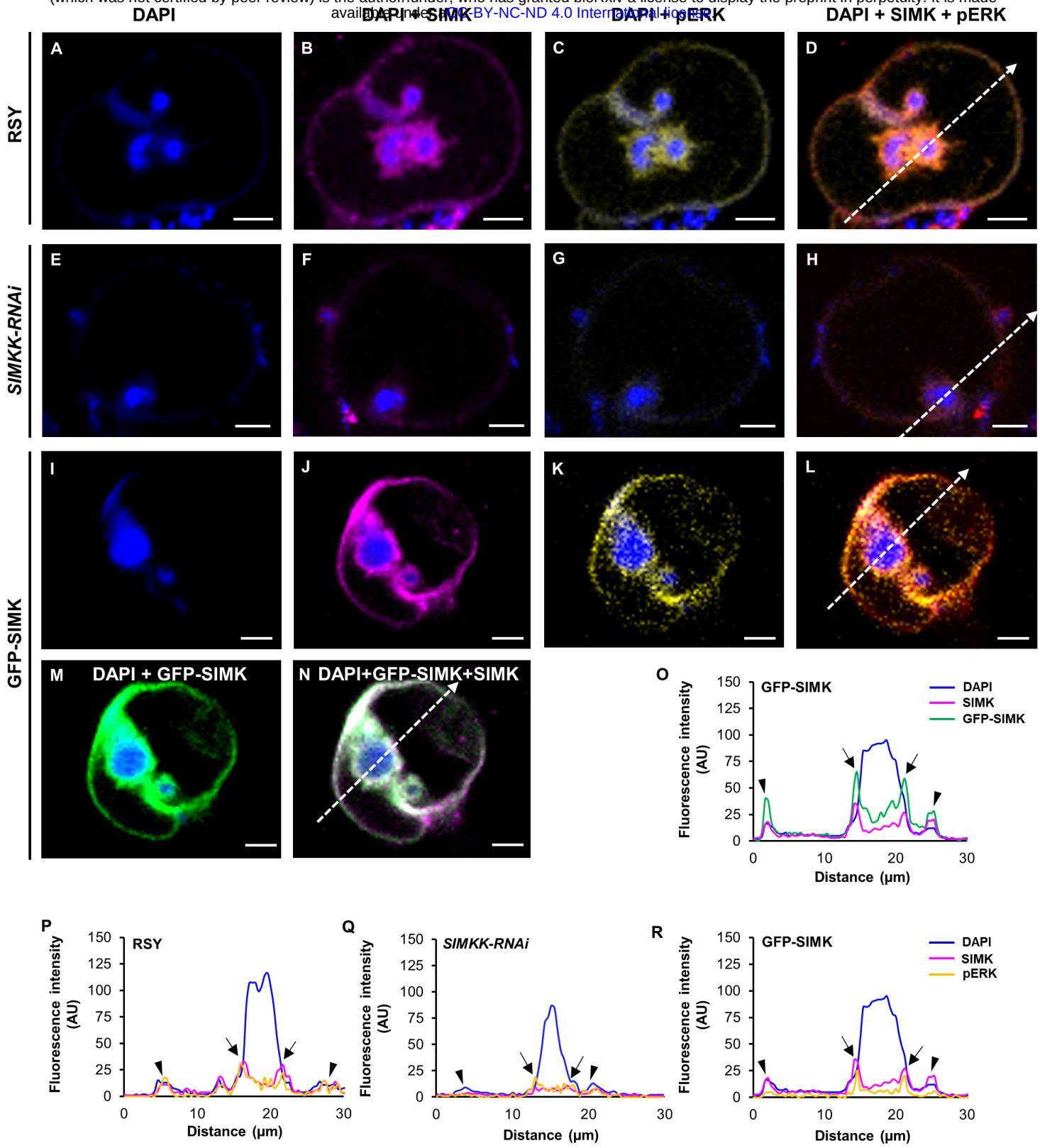

Figure 5. Subcellular immunolocalization of SIMK and activated MAPKs around infection pockets in curled root hairs after inoculation with *S. meliloti*. **(A,E,I)** Localization of DAPI-stained rhizobia inside infection pocket of RSY **(A)**, *SIMKK-RNAi* **(E)**, and GFP-SIMK **(I)** lines. **(B,F,J)** SIMK immunostained with SIMK-specific antibody and overlaid with DAPI in RSY **(B)**, *SIMKK-RNAi* **(F)**, and GFP-SIMK **(J)** lines. **(C,G,K)** Activated MAPKs immunostained with phospho-specific pERK 44/42 antibody and overlaid with DAPI in RSY **(C)**, *SIMKK-RNAi* **(G)**, and GFP-SIMK **(K)** lines. **(D,H,L)** Overlay of DAPI, SIMK and activated MAPKs in RSY **(D)**, *SIMKK-RNAi* **(H)**, and GFP-SIMK **(L)** lines. **(M,N)** GFP-tagged SIMK overlaid with DAPI **(M)** and overlay of GFP-tagged SIMK, SIMK immunostained with SIMK-specific antibody and DAPI in transgenic GFP-SIMK line **(N)**. **(O,P,Q,R)** The fluorescence intensity distribution of SIMK, activated MAPKs, GFP-tagged SIMK, and DAPI was measured along profiles indicated by white dashed arrows in **(D,H,L,N)**. Black arrows indicate the plasma membrane of the infection pocket, black arrowheads indicate the root hair plasma membrane. Scale bar = 5 μm **(A-N)**.

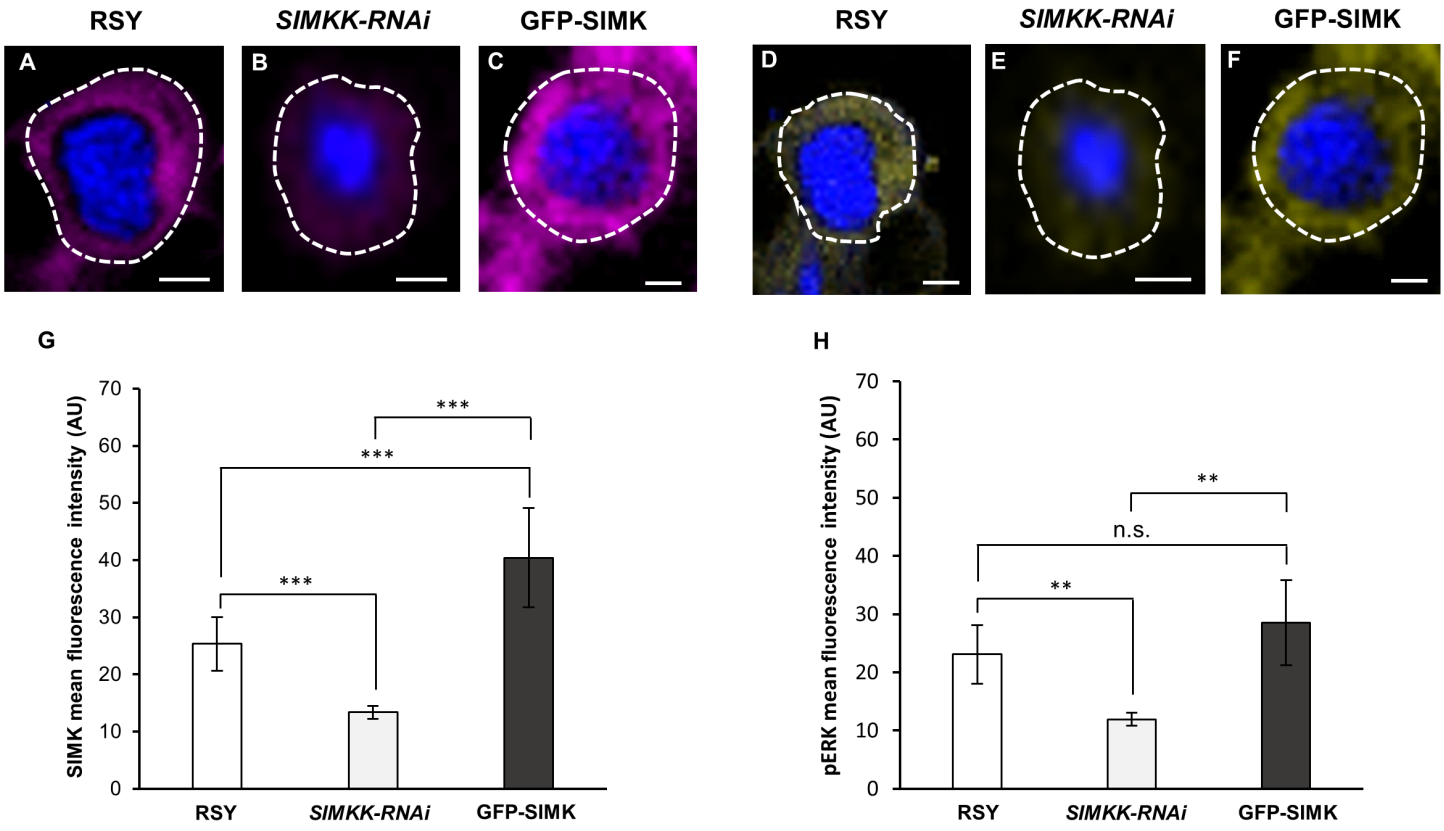

Figure 6. Quantitative analysis of SIMK and phosphorylated MAPKs fluorescence intensity distribution around infection pockets in curled root hairs after inoculation with *S. meliloti*. (A-F) Immunolocalization of SIMK **(A-C)** and phosphorylated MAPKs **(D-F)** in infection pockets of RSY **(A,D**; N=10 for SIMK, N=7 for pERK**)**, *SIMKK-RNAi* **(B,E**; N=10 for SIMK, N=7 for pERK**)**, and GFP-SIMK **(C,F**; N=9 for SIMK, N=7 for pERK**)**. White dashed lines in **(A-F)** indicate defined ROIs in which the mean fluorescence intensity was measured. **(G,H)** Quantitative evaluation of SIMK **(G)** and activated MAPKs **(H)** signal intensity in transgenic *SIMKK-RNAi* and GFP-SIMK lines compared to RSY plants. Statistical differences were calculated in Microsoft Excel using t-test. Error bars show ± standard deviation (SD). Asterisks indicate statistical significance between treatments (**p < 0,01, ***p < 0.001, n.s. no statistical significance). Scale bar = 2 µm **(A-F)**.

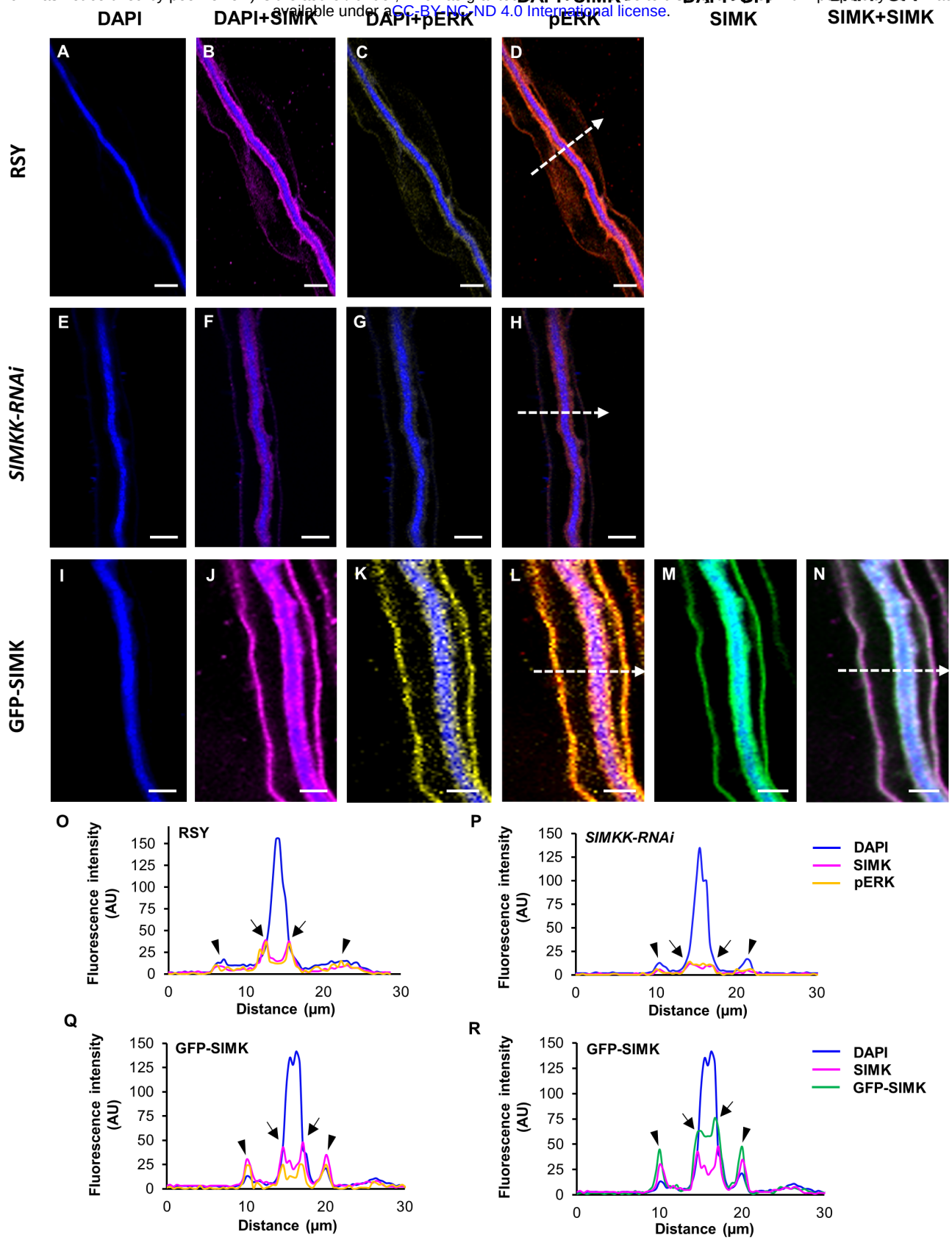

Figure 7. Subcellular immunolocalization of SIMK and activated MAPKs around ITs in root hairs induced after inoculation with *S. meliloti*. **(A,E,I)** Localization of DAPI-stained rhizobia inside ITs of RSY **(A)**, *SIMKK-RNAi* **(E)**, and GFP-SIMK **(I)** lines. **(B,F,J)** SIMK immunostained with SIMK-specific antibody and overlaid with DAPI in RSY **(B)**, *SIMKK-RNAi* **(F)**, and GFP-SIMK **(J)** lines. **(C,G,K)** Activated MAPKs immunostained with phospho-specific pERK 44/42 antibody and overlaid with DAPI in RSY **(C)**, *SIMKK-RNAi* **(G)**, and GFP-SIMK **(K)** lines. **(D,H,L)** Overlay of DAPI, SIMK and activated MAPKs in RSY **(D)**, *SIMKK-RNAi* **(H)**, and GFP-SIMK **(L)** plants. **(M,N)** GFP-tagged SIMK overlaid with DAPI **(M)** and overlay of GFP-tagged SIMK, SIMK immunostained with SIMK-specific antibody and DAPI in transgenic GFP-SIMK line **(N)**. **(O,P,Q,R)** The fluorescence intensity distribution of SIMK, activated MAPKs, GFP-tagged SIMK, and DAPI was measured along profiles indicated by white dashed arrows in **(D,H,L,N)**. Black arrows indicate the plasma membrane of IT, black arrowheads indicate the plasma membrane of root hair. Scale bar = 5 μm **(A-N)**.

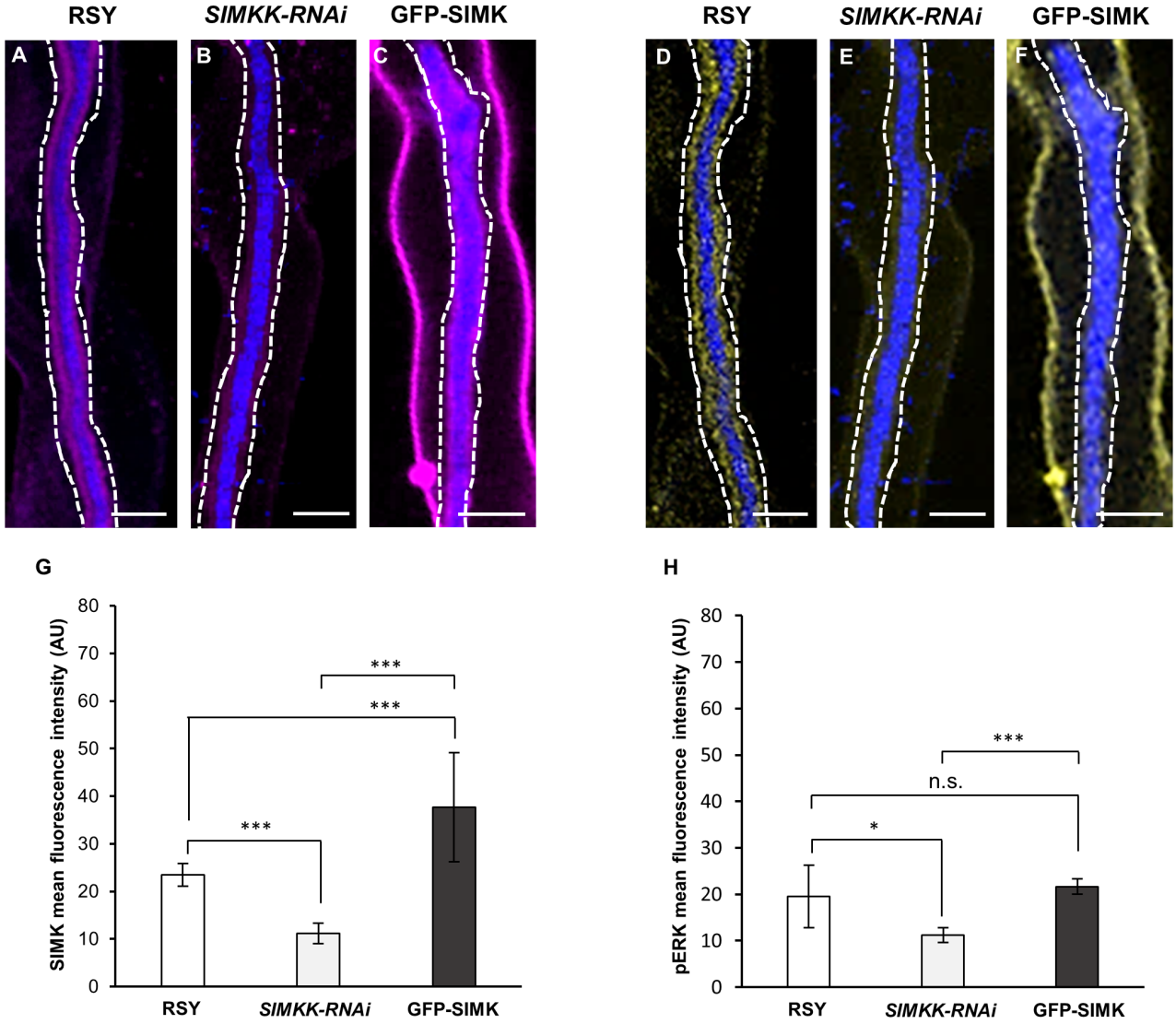

Figure 8. Quantitative analysis of SIMK and phosphorylated MAPKs fluorescence intensity distribution around ITs in root hairs after inoculation with *S. meliloti*. (A-F) Immunolocalization of SIMK **(A-C)** and phosphorylated MAPKs **(D-F)** in ITs of RSY **(A,D**; N=8 for SIMK, N=8 for pERK**)**, *SIMKK-RNAi* **(B,E**; N=6 for SIMK, N=7 for pERK**)**, and GFP-SIMK **(C,F**; N=8 for SIMK, N=8 for pERK**)**. White dashed lines in **(A-F)** indicate defined ROIs in which the mean fluorescence intensity was measured. **(G,H)** Quantitative evaluation of SIMK **(G)** and activated MAPKs **(H)** signal intensity in transgenic *SIMKK-RNAi* and GFP-SIMK lines compared to RSY plants. Statistical differences were calculated in Microsoft Excel using t-test. Error bars show ± standard deviation (SD). Asterisks indicate statistical significance between treatments (*p < 0,05, ***p < 0.001, n.s. no statistical significance). Scale bar = 5 µm **(A-F)**.

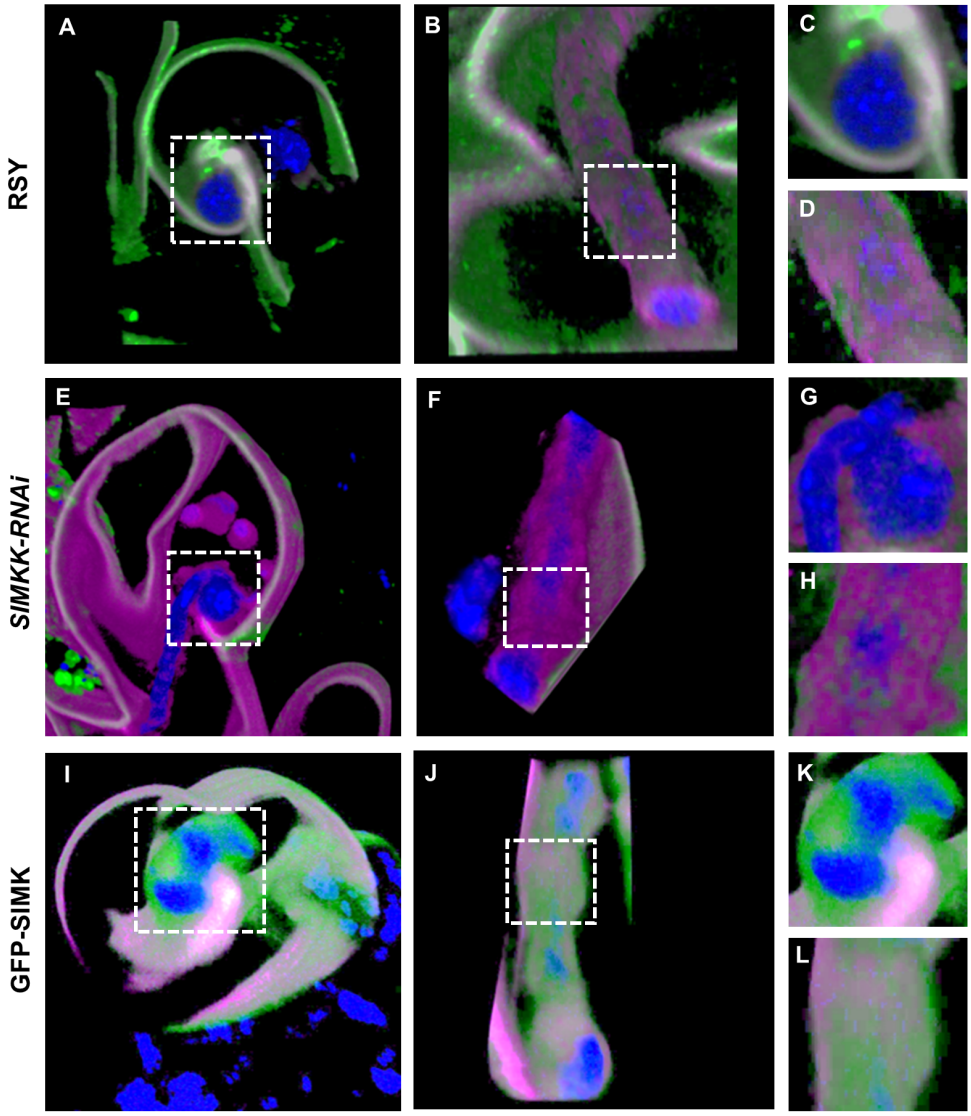

M

	Pearson's correlative coefficient	
	infection pocket	**infection thread**
RSY	0.75	0.74
SIMKK-RNAi	0.45	0.43
GFP-SIMK	0.9	0.89

Figure 9. Volume 3D rendering of rhizobia-containing early symbiotic structures with immunolabeled SIMK and membranes visualized using FM4-64FX in root hairs after inoculation with *S. meliloti*. (A-D) RSY root hairs. **(E-H)** Root hairs of *SIMKK-RNAi* line. **(I-L)** Root hairs of GFP-SIMK line. Subcellular localization of SIMK with membranes of infection pockets **(A,C,E,G,I,K)** and ITs **(B,D,F,HJ,L)**. Overlay of membranes (in magenta), SIMK (in green) and DAPI-stained rhizobia (in blue). **(M)** Averaged Pearson's correlative coefficients of colocalization analysis between SIMK and FM4-64FX-stained membranes around infection pockets and ITs. Details of infection pockets and ITs shown in **(C, D, G, H, K, L)** are marked with a white dashed boxes in **(A,B,E,F,I,J)**.

Parsed Citations

Bekešová S, Komis G, Křenek P, Vyplelová P, Ovečka M, Luptovčiak I, Šamaj J (2015) Monitoring protein phosphorylation by acrylamide pendant Phos-TagTM in various plants. Front Plant Sci 6: 336
Google Scholar: Author Only Title Only Author and Title

Bisseling T, Geurts R (2020) Specificity in legume nodule symbiosis. Science 369: 620(621
Google Scholar: Author Only Title Only Author and Title

Brewin NJ (2004) Plant cell wall remodeling in the rhizobium-legume symbiosis. Crit Rev Plant Sci 23: 293–316
Google Scholar: Author Only Title Only Author and Title

Brundrett MC (2002) Coevolution of roots and mycorrhizas of land plants. New Phytol 154: 275–304
Google Scholar: Author Only Title Only Author and Title

Cardinale F, Jonak C, Ligterink W, Niehaus K, Boller T, Hirt H (2000) Differential activation of four specific MAPK pathways by distinct elicitors. J Biol Chem 275: 36734–36740
Google Scholar: Author Only Title Only Author and Title

Cardinale F, Meskiene I, Ouaked F, Hirt H (2002) Convergence and divergence of stress-induced mitogen-activated protein kinase signaling pathways at the level of two distinct mitogen-activated protein kinase kinases. Plant Cell 14: 703–711
Google Scholar: Author Only Title Only Author and Title

Checcucci A, Azzarello E, Bazzicalupo M, Galardini M, Lagomarsino A, Mancuso S, Marti L, Marzano MC, Mocali S, Squartini A, Zanardo M, Mengoni A (2016) Mixed Nodule Infection in Sinorhizobium meliloti-Medicago sativa Symbiosis Suggest the Presence of Cheating Behavior. Front Plant Sci 7: 835
Google Scholar: Author Only Title Only Author and Title

Chen T, Zhou B, Duan L, Zhu H, Zhang Z (2017) MtMAPKK4 is an essential gene for growth and reproduction of Medicago truncatula. Physiol Plant 159: 492–503
Google Scholar: Author Only Title Only Author and Title

Chen T, Zhu H, Ke D, Cai K, Wang C, Gou H, Hong Z, Zhang Z (2012) A MAP kinase kinase interacts with SymRK and regulates nodule organogenesis in Lotus japonicus. Plant Cell 24: 823–838
Google Scholar: Author Only Title Only Author and Title

Clúa J, Roda C, Zanetti ME, Blanco FA (2018) Compatibility between Legumes and Rhizobia for the Establishment of a Successful Nitrogen-Fixing Symbiosis. Genes (Basel) 9: 125
Google Scholar: Author Only Title Only Author and Title

Costes SV, Daelemans D, Cho EH, Dobbin Z, Pavlakis G, Lockett S (2004) Automatic and quantitative measurement of protein-protein colocalization in live cells. Biophys J 86: 3993–4003
Google Scholar: Author Only Title Only Author and Title

Dénarié J, Cullimore J (1993) Lipo-oligosaccharide nodulation factors: A new class of signaling molecules mediating recognition and morphogenesis. Cell 74: 951(954
Google Scholar: Author Only Title Only Author and Title

Fåhreus G (1957) The infection of clover root hairs by nodule bacteria studied by a simple glass slide technique. J Gen Microbiol 16: 374–381
Google Scholar: Author Only Title Only Author and Title

Fournier J, Teillet A, Chabaud M, Ivanov S, Genre A, Limpens E, de Carvalho-Niebel F, Barker DG (2015) Remodelling of the infection chamber before infection thread formation reveals a two-step mechanism for rhizobial entry into the host legume root hair. Plant Physiol 167: 1233(1242
Google Scholar: Author Only Title Only Author and Title

Fournier J, Timmers AC, Sieberer BJ, Jauneau A, Chabaud M, Barker DG (2008) Mechanism of infection thread elongation in root hairs of Medicago truncatula and dynamic interplay with associated rhizobial colonization. Plant Physiol 148: 1985–1995
Google Scholar: Author Only Title Only Author and Title

Gage DJ (2004) Infection and Invasion of Roots by Symbiotic, Nitrogen-Fixing Rhizobia during Nodulation of Temperate Legumes. Microbiol Mol Biol Rev 68: 280(300
Google Scholar: Author Only Title Only Author and Title

Grimsrud PA, den Os D, Wenger CD, Swaney DL, Schwartz D, Sussman MR, Ané JM, Coon JJ (2010) Large-scale phosphoprotein analysis in Medicago truncatula roots provides insight into in vivo kinase activity in legumes. Plant Physiol 152: 19–28
Google Scholar: Author Only Title Only Author and Title

Hrbáčková M, Luptovčiak I, Hlaváčková K, Dvořák P, Tichá M, Šamajová O, Novák D, Bednarz H, Niehaus K, Ovečka M, Šamaj J

(2021) Overexpression of alfalfa SIMK promotes root hair growth, nodule clustering and shoot biomass production. Plant Biotechnol J 19: 767(784
Google Scholar: Author Only Title Only Author and Title

Ibáñez F, Wall L, Fabra A (2017) Starting points in plant-bacteria nitrogen-fixing symbioses: intercellular invasion of the roots. J Exp Bot 68: 1905–1918
Google Scholar: Author Only Title Only Author and Title

Jones KM, Kobayashi H, Davies BW, Taga, ME, Walker, GC (2007) How rhizobial symbionts invade plants: the Sinorhizobium - Medicago model. Nat Rev Microbiol 5: 619(633
Google Scholar: Author Only Title Only Author and Title

Kidaj D, Krysa M, Susniak K, Matys J, Komaniecka I, Sroka-Bartnicka A (2020) Biological activity of Nod factors. Acta Biochim Pol 67: 435(440
Google Scholar: Author Only Title Only Author and Title

Kiegerl S, Cardinale F, Siligan C, Gross A, Baudouin E, Liwosz A (2000) SIMKK, a mitogen-activated protein kinase (MAPK) kinase, is a specific activator of the salt stress-induced MAPK, SIMK. Plant Cell 12: 2247–2258
Google Scholar: Author Only Title Only Author and Title

Komis G, Šamajová O, Ovečka M, Šamaj J (2018) Cell and Developmental Biology of Plant Mitogen-Activated Protein Kinases. Annu Rev Plant Biol 69: 237(265
Google Scholar: Author Only Title Only Author and Title

Lopez-Gomez M, Sandal N, Stougaard J, Boller T (2012) Interplay of flg22-induced defence responses and nodulation in Lotus japonicus. J Exp Bot 63: 393–401
Google Scholar: Author Only Title Only Author and Title

Munnik T, Ligterink W, Meskiene I, Calderini O, Beyerly J, Musgrave A, Hirt H (1999) Distinct osmo-sensing protein kinase pathways are involved in signalling moderate and severe hyper-osmotic stress. Plant J 20: 381–388
Google Scholar: Author Only Title Only Author and Title

Oldroyd GED (2013) Speak, friend, and enter: signalling systems that promote beneficial symbiotic associations in plants. Nat Rev Microbiol 11: 252(263
Google Scholar: Author Only Title Only Author and Title

Oldroyd GED, Downie JA (2008) Coordinating nodule morphogenesis with rhizobial infection in legumes. Annu Rev Plant Biol 59: 519–46
Google Scholar: Author Only Title Only Author and Title

Oldroyd GED, Murray JD, Poole PS, Downie JA (2011) The Rules of Engagement in the Legume-Rhizobial Symbiosis. Annu Rev Genet 45: 119(144
Google Scholar: Author Only Title Only Author and Title

Ovečka M, Takáč T, Komis G, Vadovič P, Bekešová S, Doskočilová A, Smékalová V, Luptovčiak I, Šamajová O, Schweighofer A, Meskiene I, Jonak C, Křenek P, Lichtscheidl I, Škultéty Ľ, Hirt H, Šamaj J (2014) Salt-induced subcellular kinase relocation and seedling susceptibility caused by overexpression of Medicago SIMKK in Arabidopsis. J Exp Bot 65: 2335–2350
Google Scholar: Author Only Title Only Author and Title

Ovečka M, Vaškebová L, Komis G, Luptovčiak I, Smertenko A, Šamaj J (2015) Preparation of plants for developmental and cellular imaging by lightsheet microscopy. Nat Protoc 10: 1234–1247
Google Scholar: Author Only Title Only Author and Title

Ovečka M, von Wangenheim D, Tomančák P, Šamajová O, Komis G, Šamaj J (2018) Multiscale imaging of plant development by light-sheet fluorescence microscopy. Nat Plants 4: 639(650
Google Scholar: Author Only Title Only Author and Title

Ovečka M, Sojka J, Tichá M, Komis G, Basheer J, Marchetti C, Šamajová O, Kuběnová L, Šamaj J (2022) Imaging plant cells and organs with light-sheet and super-resolution microscopy. Plant Physiol 188: 683(702
Google Scholar: Author Only Title Only Author and Title

Pitzschke A (2015) Modes of MAPK substrate recognition and control. Trends Plant Sci 20: 49(55
Google Scholar: Author Only Title Only Author and Title

Poole P, Ramachandran V, Terpolilli J (2018) Rhizobia: from saprophytes to endosymbionts. Nat Rev Microbiol 16: 291(303
Google Scholar: Author Only Title Only Author and Title

Radović J, Sokolović D, Marković J (2009) Alfalfa-most important perennial forage legume in animal husbandry. Biotechnol Anim Husb 25: 465–475
Google Scholar: Author Only Title Only Author and Title

Rae AE, Rolland V, White RG, Mathesius U (2021) New methods for confocal imaging of infection threads in crop and model legumes. Plant Methods 17: 24
Google Scholar: Author Only Title Only Author and Title

Rashid MH, Krehenbrink M, Akhtar MS (2015) Nitrogen-Fixing Plant-Microbe Symbioses. In: Sustainable Agriculture Reviews (Lichtfouse, E., eds.), Springer International Publishing Switzerland 15: 193(234
Google Scholar: Author Only Title Only Author and Title

Rasmussen MW, Roux M, Petersen M, Mundy J (2012) MAP kinase cascades in Arabidopsis innate immunity. Front Plant Sci 3: 169
Google Scholar: Author Only Title Only Author and Title

Roy S, Liu W, Nandety RS, Crook A, Mysore KS, Pislariu CI, Frugoli J, Dickstein R, Udvardi MK (2020) Celebrating 20 years of genetic discoveries in legume nodulation and symbiotic nitrogen fixation. Plant Cell 32: 15(41
Google Scholar: Author Only Title Only Author and Title

Ryu H, Laffont C, Frugier F, Hwang I (2017) MAP Kinase-Mediated Negative Regulation of Symbiotic Nodule Formation in Medicago truncatula. Mol Cells 40: 17(23
Google Scholar: Author Only Title Only Author and Title

Samac DA, Austin-Phillips S (2006) Alfalfa (Medicago sativa L.). In: Agrobacterium Protocols. Methods Mol Biol. (Wang, K., ed.) Clifton, N. J.: Humana Press, 301–312
Google Scholar: Author Only Title Only Author and Title

Šamaj J, Ovečka M, Hlavacka A, Lecourieux F, Meskiene I, Lichtscheidl I, Lenart P, Salaj J, Volkmann D, Bögre L, Baluska F, Hirt H (2003) Involvement of MAP kinase SIMK and actin cytoskeleton in the regulation of root hair tip growth. Cell Biol Int 27: 257(259
Google Scholar: Author Only Title Only Author and Title

Šamaj J, Ovečka M, Hlavacka A, Lecourieux F, Meskiene I, Lichtscheidl I, Lenart P, Salaj J, Volkmann D, Bögre L, Baluška F, Hirt H (2002) Involvement of the mitogen-activated protein kinase SIMK in regulation of root hair tip growth. EMBO J 21: 3296(2306
Google Scholar: Author Only Title Only Author and Title

Šamajová O, Plíhal O, Al-Yousif M, Hirt H, Šamaj J (2013) Improvement of stress tolerance in plants by genetic manipulation of mitogen-activated protein kinases. Biotechnol Adv 31: 118–128
Google Scholar: Author Only Title Only Author and Title

Shaw SL, Long SR (2003) Nod factor inhibition of reactive oxygen efflux in a host legume. Plant Physiol 132: 2196–2204
Google Scholar: Author Only Title Only Author and Title

Smékalová V, Doskočilová A, Komis G, Šamaj J (2014) Crosstalk between secondary messengers, hormones and MAPK modules during abiotic stress signalling in plants. Biotechnol Adv 32: 2(11
Google Scholar: Author Only Title Only Author and Title

Sprent JI (2008) 60Ma of legume nodulation. What's new? What's changing? J Exp Bot 59: 1081–1084
Google Scholar: Author Only Title Only Author and Title

Sprent JI, James E (2007) Legume evolution: Where do nodules and mycorrhizas fit in? Plant Physiol 144: 575–581

Sun T, Zhang Y (2022) MAP kinase cascades in plant development and immune signaling. EMBO Rep 23: e53817
Google Scholar: Author Only Title Only Author and Title

Terpolilli JJ, Hood GA, Poole PS (2012) What determines the efficiency of N2-fixing Rhizobium-Legume Symbioses. Adv Microb Physiol 60: 325–389
Google Scholar: Author Only Title Only Author and Title

Tichá M, Hlaváčková K, Hrbáčková M, Ovečka M, Šamajová O, Šamaj J (2020) Super-resolution imaging of microtubules in Medicago sativa. Methods Cell Biol 160: 237(251
Google Scholar: Author Only Title Only Author and Title

Timmers ACJ (2008) The role of the plant cytoskeleton in the interaction between legumes and rhizobia. J Microsc 231: 247(256
Google Scholar: Author Only Title Only Author and Title

Vyplelová P, Ovečka M, Komis G, Šamaj J (2018) Advanced microscopy methods for bioimaging of mitotic microtubules in plants. Methods in Cell Biology 145: 129(158
Google Scholar: Author Only Title Only Author and Title

Walker L, Lagunas D, Gifford ML (2020) Determinants of Host Range Specifity in Legume-Rhizobia Symbiosis. Front Microbiol 11: 585749
Google Scholar: Author Only Title Only Author and Title

Wang Q, Liu J, Zhu H (2018) Genetic and molecular mechanisms underlying symbiotic specificity in legume-rhizobium interactions. Front Plant Sci 9: 313

Google Scholar: Author Only Title Only Author and Title

White J, Prell J, James EK, Poole P (2007) Nutrient sharing between symbionts. Plant Physiol 144: 604–614

Google Scholar: Author Only Title Only Author and Title

Xu J, Zhang S (2015) Mitogen-activated protein kinase cascades in signaling plant growth and development. Trends Plant Sci 20: 56(64

Google Scholar: Author Only Title Only Author and Title

Yan Z, Cao J, Fan Q, Chao H, Guan X, Zhang Z, Duanmu D (2020) Dephosphorylation of LjMPK6 by phosphatase LjPP2C is involved in regulating nodule organogenesis in Lotus japonicus. Int J Mol Sci 21: 5565.

Google Scholar: Author Only Title Only Author and Title

Yang J, Lan L, Jin Y, Yu N, Wang D, Wang E (2022) Mechanisms underlying legume-rhizobium symbioses. J Integr Plant Biol 64: 244(267

Google Scholar: Author Only Title Only Author and Title

Yin J, Guan X, Zhang H, Wang L, Li H, Zhang Q, Chen T, Zeyuan X, Hong Z, Cao Y, Zhang Z (2019) An MAP kinase interacts with LHK1 and regulates nodule organogenesis in Lotus japonicus. Sci China Life Sci 62: 1203–1217

Google Scholar: Author Only Title Only Author and Title

Zhang M, Zhang S (2022) Mitogen-activated protein kinase cascades in plant signaling. J Integr Plant Biol 64: 301– 341

Google Scholar: Author Only Title Only Author and Title